NASA Technical Memorandum 4135

Results of Aircraft Open-Loop Tests of an Experimental Magnetic Leader Cable System for Guidance During Roll-Out and Turnoff

W. Thomas Bundick, David B. Middleton,
and William L. Poole
Langley Research Center
Hampton, Virginia

National Aeronautics and
Space Administration
Office of Management
Scientific and Technical
Information Division

1990

Summary

An experimental magnetic leader cable (MLC) system designed to measure aircraft lateral displacement from centerline and heading relative to centerline during roll-out, turnoff, and taxi was tested at NASA's Wallops Flight Facility. The MLC system consisted of ground equipment that produced a magnetic field along the runway centerline and equipment in the aircraft that detected the strength and direction of this field. The ground subsystem included closed-loop electrical cables that were buried along the centerline of a runway, its high-speed turnoff, and taxiway. The aircraft subsystem consisted of three orthogonal coils, a preamplifier, and an analog chassis that were installed on NASA's Transport System Research Vehicle (TSRV), a modified Boeing 737. Output voltages from the analog chassis were recorded on magnetic tape, and digital processing of these signals to compute estimates of displacement and heading was accomplished postflight. This processing would be done in the flight computer in normal operation. For flexibility in testing, the experimental equipment was designed to operate at a frequency of either 150 Hz or 990 Hz with either a wideband filter or a narrowband filter at each frequency.

Static tests were conducted with the aircraft parked on the runway at various displacements from and parallel to the cable. Dynamic tests were conducted with the pilot taxiing the aircraft under manual control along the runway, turnoff, and taxiway. In posttest processing, two estimates of displacement were computed using different algorithms. Estimates of heading also were computed.

Results of these tests indicate that estimates of aircraft displacement from centerline from either of the two algorithms appear to be adequate for use by an automatic control system during roll-out, turnoff, and taxi. Estimates of heading, however, are not sufficiently accurate for use, probably because of distortion of the magnetic field by the metal aircraft, and heading must be obtained from another source if it is required. Electromagnetic interference from the aircraft power system made estimates obtained with the 990-Hz wideband filter unusable, but the interference was adequately suppressed by the other filters. In general, performance was better at 150 Hz than at 990 Hz.

The MLC system performed sufficiently well in estimating lateral displacement to warrant future closed-loop testing of an automatic roll-out and turnoff system that uses the MLC lateral displacement estimates for guidance.

Introduction

To accommodate the expected increase in future air traffic, the landing rate at major airports must be increased. Advanced avionics, advanced air traffic control techniques, increased understanding of wake vortices, and the new Microwave Landing System (MLS) have the potential to increase runway landing rate by decreasing the spacing between landing aircraft. Increasing the landing rate, however, demands that runway occupancy time be decreased; that is, landing aircraft must be cleared from the runway more rapidly. One technique for reducing runway occupancy time is the use of high-speed turnoffs. Safe and efficient use of high-speed turnoffs requires the availability of turnoff guidance, particularly for use with automatic controls. Clearly, if the MLS and high-speed turnoffs are to be used to their peak potential, appropriate guidance information during turnoff and taxi must be available.

The azimuth and DME (distance measuring equipment) functions of the MLS provide some lateral and longitudinal guidance, or position information, during roll-out; but this information is not sufficiently accurate during turnoff and may not be available during taxi. Obviously, visual guidance can be used by the pilot for manual control during good visibility. However, visual guidance may not be adequate during poor visibility conditions, and during any conditions it is not available to the automatic control system.

One potential source of guidance during roll-out, turnoff, and taxi is the magnetic leader cable (MLC). An electrical cable would be buried in the runway, turnoff, and taxiway along the path the aircraft is to follow (normally, the centerline), as illustrated in figure 1. An audio-frequency current is passed through the cable, setting up a magnetic field. A sensor in the aircraft detects this magnetic field and provides guidance information to the pilot and/or automatic control system. The MLC would supplement the MLS by providing an independent guidance signal during roll-out and turnoff and by providing guidance during taxi in areas of the airfield outside of MLS coverage.

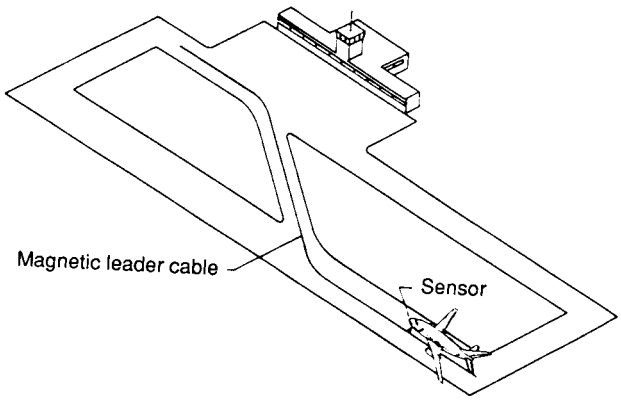

Figure 1. Roll-out and turnoff guidance with magnetic leader cable.

The magnetic leader cable was investigated by the British (refs. 1 and 2) as early as the 1950's as a source of guidance during final approach and landing, but it was never adopted as an operational system. One factor limiting its usefulness in that application was the difficulty in obtaining accurate guidance during final approach. This limitation would not be a factor in the current concept because MLS guidance would be used during final approach, and the MLC would not be used before touchdown.

Work on the MLC has been revived as part of the NASA Advanced Transport Operating System (ATOPS) program. One facet of this effort involved the development of a concept and algorithms for the automatic control of the aircraft during roll-out and turnoff using MLS and MLC guidance information. Portions of this work were performed under contract to NASA and have been reported in references 3 and 4.

A second facet of the MLC work has been the development of a sensor, or aircraft subsystem. One portion of this development was the analysis of the the effects of cable geometry and aircraft attitude on the accuracy of the MLC system (ref. 5). The major portion of the sensor development work has been the installation of a leader cable at the Wallops Flight Facility and the design, fabrication, and field testing of an aircraft subsystem. Initial testing was accomplished using an analog breadboard sensor based on a design by Ohio State University. This equipment was installed in a van and tested at Wallops with a temporary cable (ref. 6). The aircraft subsystem was redesigned to provide a digital implementation of the computations in the MLC algorithms, and additional van tests with the hybrid analog/digital subsystem were performed at Wallops with a more permanent MLC ground installation. Results of all these tests indicated that (1) an MLC system has the potential to provide guidance information in the form of a measure of the lateral displacement of the aircraft from the cable during roll-out, turnoff, and taxi; (2) the relative heading information provided by the MLC is probably not useful because of the distortion of the magnetic field by the metal aircraft; and (3) electromagnetic interference from other aircraft systems needs further investigation.

More recently the analog portion of the aircraft subsystem was installed in the NASA TSRV (a modified Boeing 737), and tests with the aircraft were performed at the Wallops Flight Facility to evaluate the capability of the MLC system to provide guidance information to an aircraft during roll-out, turnoff, and taxi. The tests were open loop; that is, the aircraft was guided manually by the pilot, not automatically by the MLC. These tests are the subject of this report. A brief review of the theory of operation of the MLC concept will be presented first, followed by a description of the test equipment and test procedures. Then, the test results will be presented and will be followed by conclusions.

Symbols

A_x, A_y, A_z	area of surface bounded by x-, y-, and z-coil, respectively, m^2
$\mathbf{B}$	magnetic induction field, Wb/m^2
B_x, B_y, B_z	Cartesian components of $\mathbf{B}$, Wb/m^2
$d\mathbf{l}$	incremental length along the closed contour C, m
E	sum of squared error between theoretical and measured voltages, V^2
$G_x, G_{xs}, G_y, G_z, G_{zs}$	voltage gain of x-, xs-, y-, z-, and zs-channel, respectively, including the coil, $\mu_o \omega N A / 2\pi$
g_x, g_y, g_z	voltage gain of x-, y-, and z-channel, respectively, excluding the coil
$\mathbf{H}$	magnetic intensity, A/m
H	magnitude of $\mathbf{H}$, A/m
H_x, H_y, H_z	Cartesian components of $\mathbf{H}$, A/m
I	rms current in cable, A
$\mathbf{i}_\theta$	unit vector in θ-direction in cylindrical coordinates
$\mathbf{i}_1$, $\mathbf{i}_2$, $\mathbf{i}_3$	unit vector perpendicular to plane of the x-, y-, and z-coil, respectively
k_{y_2}	calibration factor relating estimate $\hat{y}_2$ to voltage ratio $\left(\frac{V_z}{V_y^2+V_z^2}\right)$, m
N_x, N_y, N_z	number of turns in the x-, y-, and z-coil, respectively
Q	filter quality factor (filter center frequency divided by the half-power bandwidth)
t	time, sec
$V_x, V_{xs}, V_y, V_z, V_{zs}$	dc output voltage in the x-, xs-, y-, z-, and zs-channel, respectively, V
x	position of coils along cable, m or ft
y, y_{true}	lateral displacement of coils from cable, m or ft
$\hat{y}_1$, $\hat{y}_2$	estimate of the displacement y from equation (6) or (10), respectively (in analysis of experimental data used magnitude of V_z and sign of V_{zs}), m or ft
$\hat{y}_{1s}$, $\hat{y}_{2s}$	estimate of the displacement y from equation (6) or (10), respectively (in analysis of experimental data used magnitude of V_{zs}), m or ft
z	height of coils above cable, m or ft
θ	angular coordinate in cylindrical coordinates, rad
μ_o	permeability of free space, $4\pi \times 10^{-7}$ Wb/A-m
ρ	radial coordinate in cylindrical coordinates, m
Ψ	heading relative to cable, rad or deg
ω	angular frequency of current in cable, rad/sec
Subscripts:	
i	denotes ith data point
s	denotes signal in channel containing synchronous detector

Superscripts:

ˆ	denotes estimated value

Abbreviations:

ac	alternating current
ATOPS	Advanced Transport Operating System
AWG	American Wire Gauge
dc	direct current
EMI	electromagnetic interference
MLC	magnetic leader cable
MLS	microwave landing system
std. dev.	standard deviation
TSRV	Transport System Research Vehicle
UHF	ultrahigh frequency
VHF	very high frequency

Theory of Operation

A detailed development of the theory of the MLC is contained in reference 5, and only a brief discussion is presented here. Consider an infinitely long, straight conductor coincident with the x-axis carrying a current I, as depicted in figure 2. The MLC utilizes a sinusoidal current in the audio-frequency range. Because of the extremely long wavelengths and short distances involved, the propagation time can be neglected. Thus, to simplify the mathematics, the time dependence of the current and resulting magnetic field is omitted.

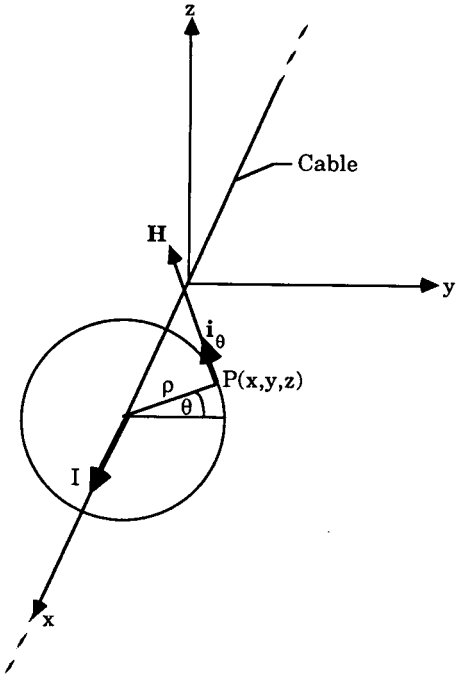

Figure 2. Geometry for infinite straight cable.

Returning now to figure 2, the magnetic intensity $\mathbf{H}$ at point $P(x, y, z)$ can be computed with Ampere's circuital law as follows:

$$\int_C \mathbf{H} \cdot d\mathbf{l} = I \tag{1}$$

Because the field is uniformly symmetrical about the conductor, equation (1) can be solved to give

$$\mathbf{H} = \frac{I}{2\pi\rho}\mathbf{i}_\theta \tag{2}$$

In Cartesian coordinates, equation (2) becomes

$$H_x = 0 \tag{3a}$$

$$H_y = -H \sin\theta = -\frac{I}{2\pi}\frac{z}{y^2 + z^2} \tag{3b}$$

$$H_z = H \cos\theta = \frac{I}{2\pi}\frac{y}{y^2 + z^2} \tag{3c}$$

Suppose that there are three mutually orthogonal coils located at point P such that the axes $\mathbf{i}_1$, $\mathbf{i}_2$, and $\mathbf{i}_3$ (perpendicular to the planes of the coils) are parallel to the coordinate axes x, y, and z, respectively. The magnitude of the voltage V_x induced in the x-coil by the magnetic field $\mathbf{B}$ and amplified by the sensor electronics is

$$V_x = \omega N_x A_x B_x g_x \tag{4}$$

where

$$\mathbf{B} = \mu_o \mathbf{H}, \text{ Wb/m}^2$$

Combining equations (3a) and (4) gives

$$V_x = 0 \tag{5a}$$

Similarly for the y- and z-coils,

$$V_y = \omega N_y A_y B_y g_y = \frac{-\mu_o \omega N_y A_y I g_y}{2\pi}\frac{z}{y^2 + z^2} = -\frac{zIG_y}{y^2 + z^2} \tag{5b}$$

$$V_z = \omega N_z A_z B_z g_z = \frac{\mu_o \omega N_z A_z I g_z}{2\pi}\frac{y}{y^2 + z^2} = -\frac{yIG_z}{y^2 + z^2} \tag{5c}$$

Take the ratio of the voltages V_z to V_y and solve for y, thereby obtaining an estimate $\hat{y}_1$ of y.

$$\hat{y}_1 = -\frac{zG_y}{G_z}\frac{V_z}{V_y} \tag{6}$$

Thus, the estimate $\hat{y}_1$ of the displacement y of the coils from the MLC is obtained by measuring the amplified coil voltages V_y and V_z and using equation (6). Under the assumptions inherent in equation (6) (infinite straight wire in free space), the accuracy of the estimate depends on the accuracy of the knowledge of the gains G_y and G_z and on the error in measuring the voltages V_y and V_z due to noise and interference. Note that the estimate $\hat{y}_1$ is a linear function of the ratio V_z/V_y and that knowledge of the coil height z is required, but knowledge of the current I is not. Of course, the magnitude of the current I is important in determining the signal-to-noise ratio of the voltages V_y and V_z.

If the gains G_y and G_z are equal, the displacement y of the coils can be determined by an alternative algorithm that requires knowledge of the current I, but not of the height z. This can be

seen by finding the ratio $V_z/(V_y^2 + V_z^2)$ as follows:

$$\frac{V_z}{V_y^2 + V_z^2} = \frac{2\pi N_z A_z g_z}{\mu_o \omega I} \frac{y(z^2 + y^2)}{N_y^2 A_y^2 g_y^2 z^2 + N_z^2 A_z^2 g_z^2 y^2} \tag{7}$$

Now, if $N_y A_y g_y = N_z A_z g_z$, equation (7) becomes

$$\frac{V_z}{V_y^2 + V_z^2} = \frac{2\pi y}{\mu_o \omega I N_y A_y g_y} \tag{8}$$

Equation (8) can be solved for y to obtain another estimate $\hat{y}_2$ of displacement

$$\hat{y}_2 = \frac{\mu_o \omega I N_y A_y g_y}{2\pi y} = \frac{V_z}{V_y^2 + V_z^2} = k_{y_2} \frac{IV_z}{V_y^2 + V_z^2} \tag{9}$$

where k_{y_2} is a calibration factor. Note that this expression is a linear function of $V_z/(V_y^2 + V_z^2)$. If the y- and z-channel gains are not equal, an estimate of y can be found from

$$\hat{y}_2 = \frac{IG_z V_z}{\left(\frac{G_z}{G_y} V_y\right)^2 + V_z^2} \tag{10}$$

Suppose now that the coils are rotated in the xy-plane such that $\mathbf{i}_1$ makes an angle Ψ with the x-axis, as shown in figure 3. The voltage output V_z of the z-channel remains the same as in equation (5c), but the voltages V_x and V_y become

$$V_x = \omega N_x A_x B_y g_x \sin \Psi = \frac{-\mu_o \omega N_x A_x I g_x}{2\pi} \frac{z}{y^2 + z^2} \sin \Psi = -\frac{zIG_x}{y^2 + z^2} \sin \Psi \tag{11a}$$

$$V_y = \omega N_y A_y B_y g_y \cos \Psi = \frac{-\mu_o \omega N_y A_y I g_y}{2\pi} \frac{z}{y^2 + z^2} \cos \Psi = -\frac{zIG_y}{y^2 + z^2} \cos \Psi \tag{11b}$$

where Ψ is the aircraft heading relative to the cable. Taking the ratio V_x/V_y gives

$$\frac{V_x}{V_y} = \frac{N_x A_x g_x}{N_y A_y g_y} \tan \Psi = \frac{G_x}{G_y} \tan \Psi \tag{12}$$

If the angle Ψ is small, $\tan \Psi$ can be approximated by Ψ, and equation (12) can be solved for an estimate $\hat{\Psi}$ of the aircraft heading

$$\hat{\Psi} \approx \frac{G_y}{G_x} \frac{V_x}{V_y} \tag{13}$$

Note that in this equation the estimate $\hat{\Psi}$ is a linear function of the ratio V_x/V_y. Equation (6) for the displacement now becomes

$$\hat{y}_1 = -\frac{zG_y}{G_z} \frac{V_z}{V_y} \cos \Psi \tag{14}$$

However, if Ψ is small, equation (14) can be approximated by equation (6).

We have shown conceptually that for an infinitely long, straight cable carrying a current I, the lateral displacement y (relative to the cable) of a set of three mutually orthogonal coils can be determined by measuring the voltage outputs of the appropriate coils and processing these measurements with either of two algorithms. One of the algorithms (eq. (6)) requires that the height z of the coils be known, whereas the other algorithm (eq. (10)) requires that the current I in the cable be known. Furthermore, the angle of rotation Ψ of the coils in the xy-plane can be determined by using the coil voltages and processing them with a third algorithm (eq. (13)).

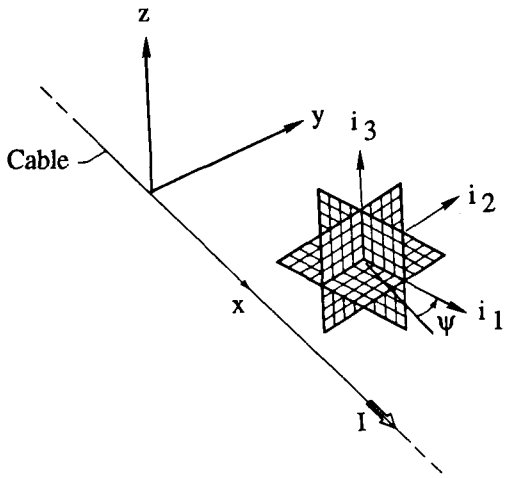

Figure 3. Coil geometry.

Conceptually it follows that, if the coils are rigidly attached to an aircraft and the magnetic cable is laid on the runway centerline, the sensor can be used to measure the displacement of the aircraft from centerline and the heading of the aircraft relative to centerline. An experimental sensor system was designed to evaluate this concept with these algorithms.

Experimental Equipment

Ground Subsystem

A semipermanent MLC ground subsystem was installed on runway 22 and the high-speed turnoff at Wallops Flight Facility. As shown in figure 4, two cables were installed. The first cable followed the centerline for the entire length of the runway, and the second cable followed the centerline from the approach end to the turnoff, along the turnoff onto the taxiway, and along the taxiway to its end. The return wires to complete the loops were buried in a common trench several hundred feet to the side of the runway. On the runway and taxiway the cable was placed in a groove cut in the concrete or asphalt surface to a depth of 0.5 to 1.0 in. and covered with a mastic material. Some problems were experienced with the cable rising to the surface through the mastic, probably as a result of thermal expansion and contraction of the concrete and the wire. The cable was AWG #12 stranded copper, and the total resistance of each loop was on the order of 33 ohms.

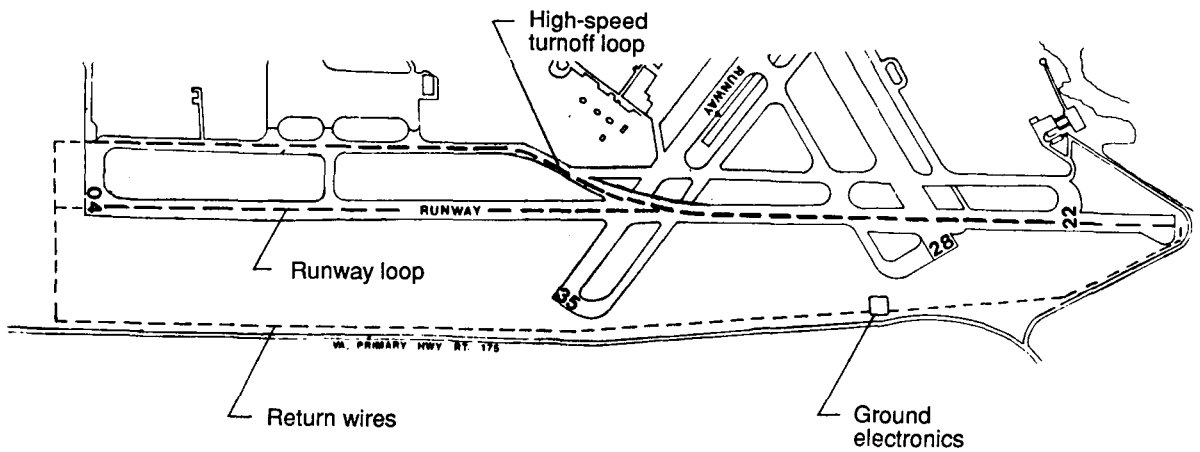

Figure 4. MLC installation at Wallops Flight Facility.

The ground electronics, shown schematically in figure 5, consisted of an audio-frequency power source, an ammeter, and a switch to select the runway loop or the turnoff loop. The power source included a self-contained oscillator and a frequency meter and was capable of providing 1 kVA in the frequency range of 20 Hz to 2 kHz. This power capability was more than adequate to supply the cable with the 2 A or less of current required for any of the tests.

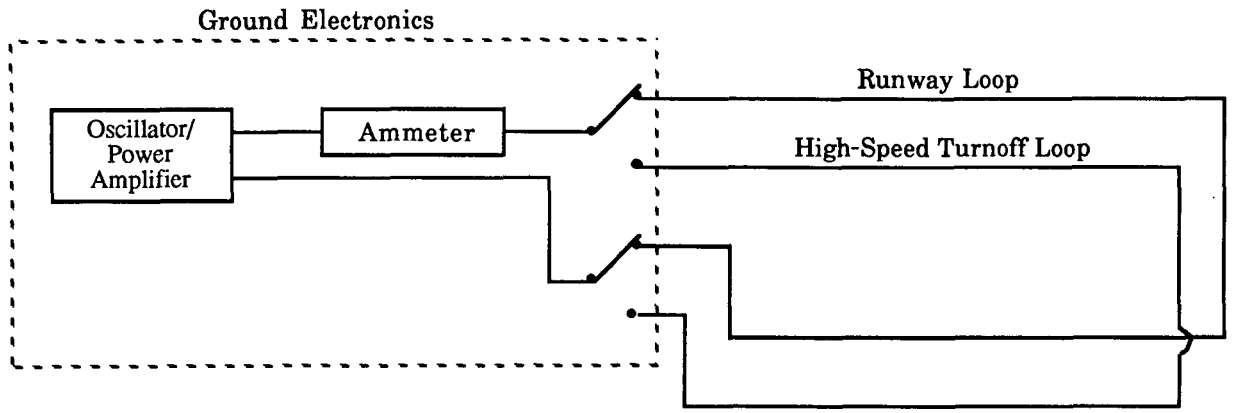

Figure 5. Block diagram of MLC ground equipment.

Aircraft Subsystem

The aircraft subsystem consisted of three orthogonal coils, a preamplifier, and the analog chassis, as shown in block diagram form in figure 6. The three coils were wound on a 4-in. wooden cube using 215 to 400 turns of AWG #32 solid copper wire. The number of turns in each coil was chosen to compensate for the three coils each having different enclosed areas, since they were wound one inside the other on the same cube. The preamplifier provided amplification and some low-pass filtering ahead of the cable run to the analog chassis. The analog chassis supplied dc power to the preamplifier. The analog chassis provided further amplification, bandpass filtering, and detection of the ac signals, whose frequency is that of the cable current. By detection is meant the conversion of the ac signal, whose amplitude is a function of the lateral displacement from the cable, to a dc signal, as in the detection or demodulation of AM (amplitude modulated) signals. Thus, the dc signal amplitude is a function of the lateral displacement and varies as this displacement changes.

To provide the flexibility in the experimental equipment for conducting tests to evaluate the effects of cable current frequency and the effects of noise and electromagnetic interference, the analog chassis was designed and fabricated with four switch-selectable bandpass filters in each of the three channels. Two of the filters had a center frequency of 150 Hz, and two had a center frequency of 990 Hz. At each center frequency, one filter (wideband) was a Bessel design with a Q of 5, and the other (narrowband) was a Chebychev design with a Q of 20. These filters were implemented using universal active filter integrated circuits. An earlier design had used a center frequency of 165 Hz, but this was changed to 150 Hz to reduce interference from the third harmonic of 60-Hz power.

The detector in each channel was simply a half-wave rectifier (diode detector) with low-pass filtering. In addition, synchronous detectors were included in the x- and z-channels with the reference signal being the y-channel signal. The synchronous detectors were necessary to preserve the 0° or 180° phase relationship between the y- and x- channels and between the y- and z-channels. This phase relationship (same sign or opposite sign in the dc signals after detection) was required to distinguish whether the heading and displacement estimates were to the right or the left of the cable. The dc output signals were fed to the flight data system for recording. In normal operation of the MLC, these signals would be processed in real time by the flight computer using equations (6), (10), and (13) to obtain estimates of the aircraft heading and lateral displacement. Since the flight

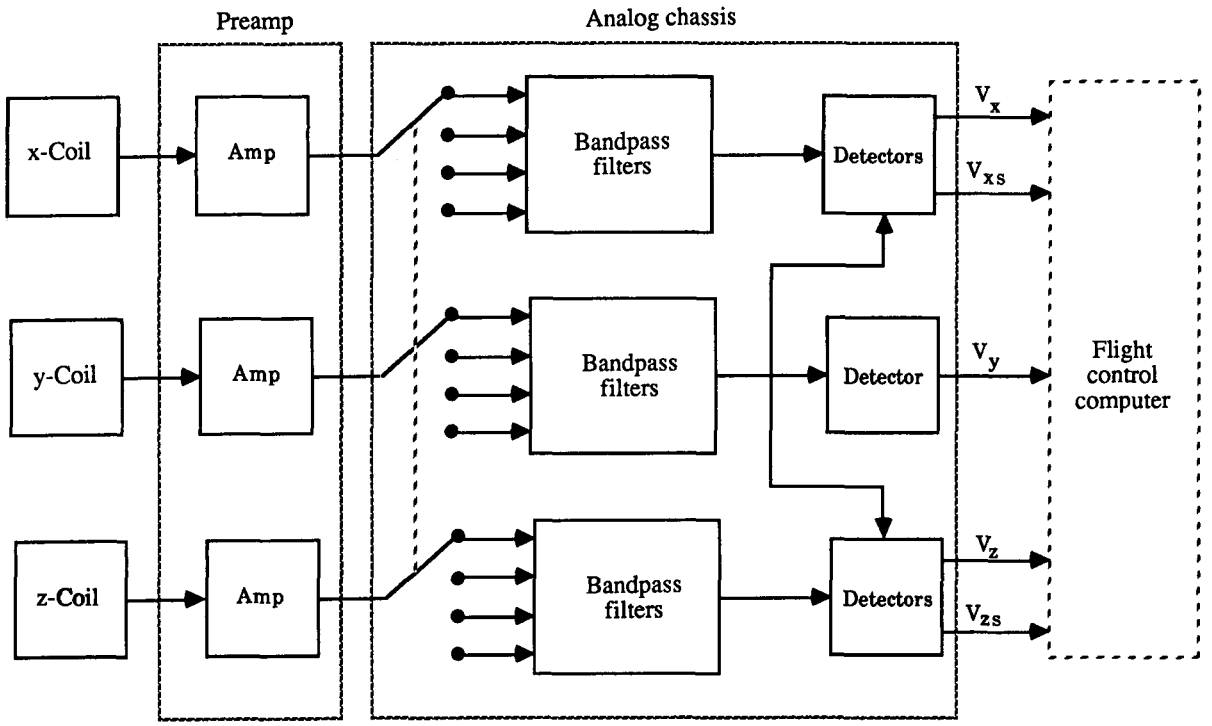

Figure 6. Simplified block diagram of aircraft subsystem.

control system would not utilize these estimates in the open-loop tests, this processing was done postflight with the same algorithms.

The coils and preamplifier were mounted in the nose of the Boeing 737 under the radome at a height of approximately 7 ft above the runway. A photograph of the installation is shown in figure 7. The analog chassis was mounted in a rack in the cabin as shown in figure 8.

Test Results

Static Tests

For the static tests, the TSRV aircraft was positioned on the runway at the desired lateral displacement from the cable by using a tug and was aligned as near parallel to the cable as practical. At displacements of −25, 0, 6, 12, 25, and 50 ft, data were taken at each of the four frequency/bandwidth combinations by measuring the dc voltages V_x, V_{xs}, V_y, V_z, and V_{zs} out of the analog chassis with a digital voltmeter. In addition, at displacements of 0, 25, and 50 ft these five voltage outputs were recorded on magnetic tape at a rate of 20 samples/second for approximately 30 sec at each frequency/bandwidth combination. In subsequent discussions of the analysis of the static test data, the data recorded during each of these 30-sec periods will be referred to as a block of data.

Voltage measurements. From equation (5b) it was expected that the y-channel voltage V_y from the analog chassis would be described by

$$V_y = -\frac{zIG_y}{y^2 + z^2} \tag{5b}$$

where the gain G_y is unknown. To find an estimate of the y-channel gain when using the 150-Hz low-Q filter, a least squares fit of the theoretical expression in equation (5b) to the V_y data taken with that filter was performed. The V_y data used were the six voltmeter measurements taken at the

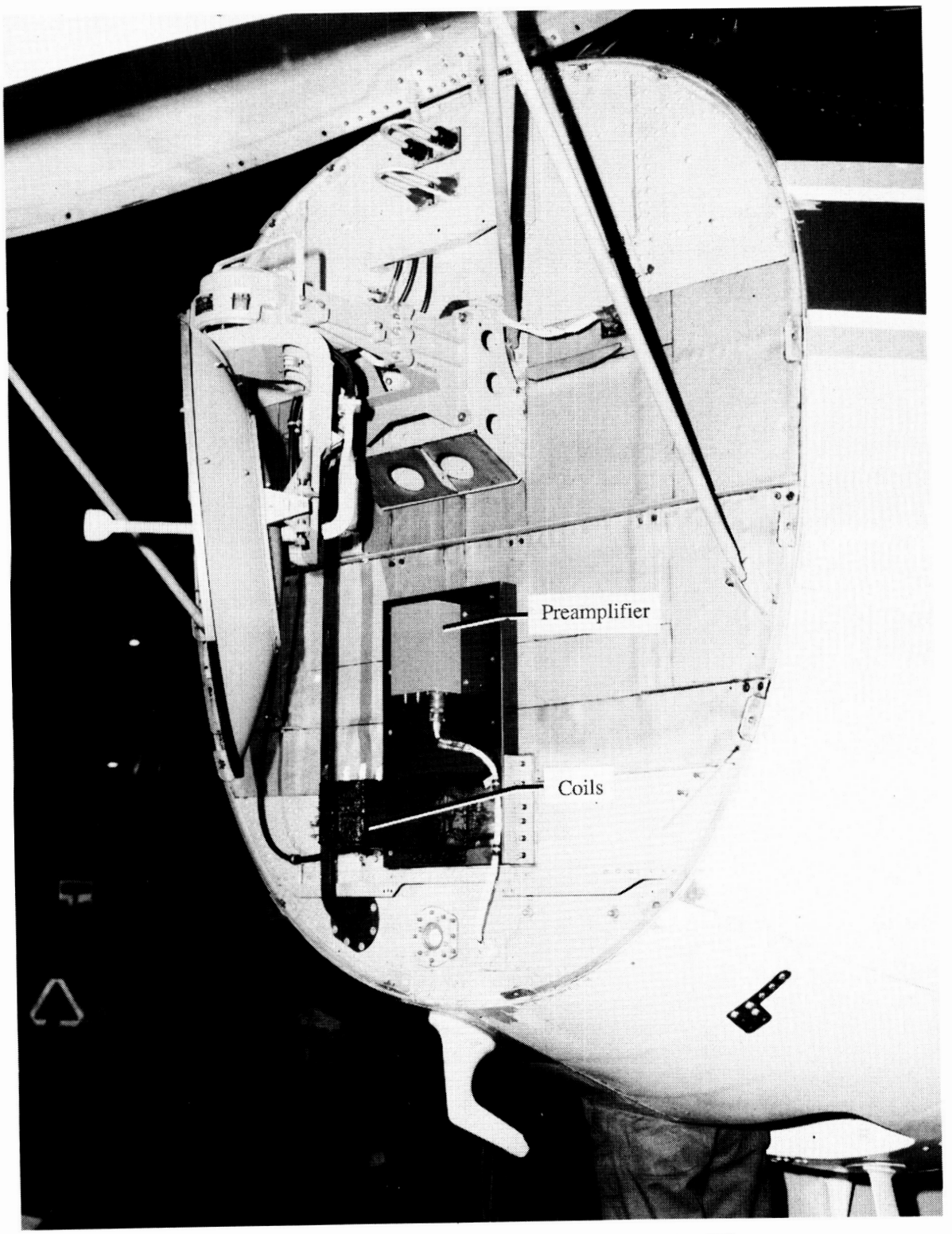

Figure 7. Coils and preamplifier installed in nose of Boeing 737.

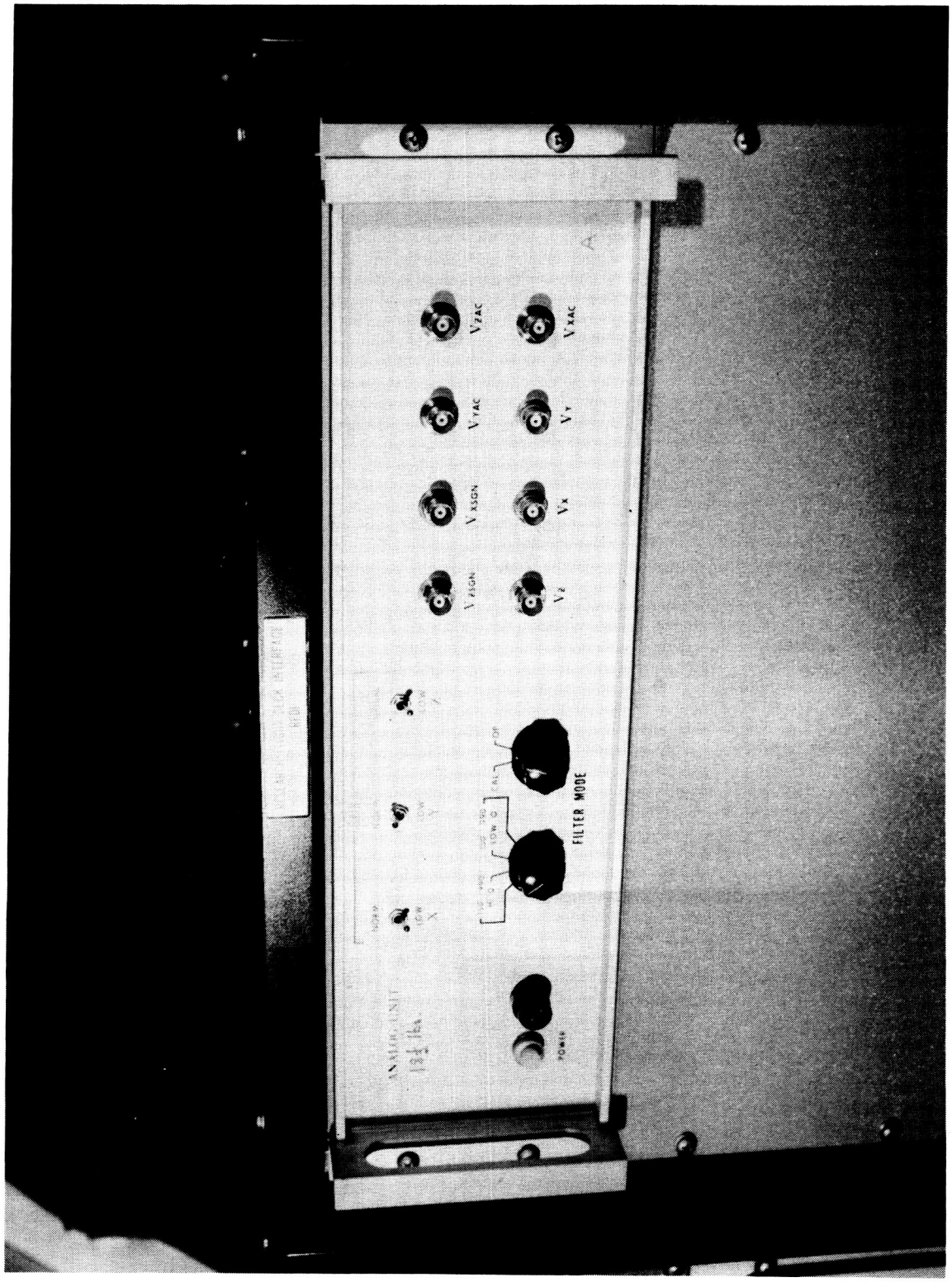

Figure 8. Analog chassis installed in Boeing 737.

six different values of y. The sum of the squared error between the measured data and the theoretical data is given by

$$E = \sum_i \left[V_{y_i} - \frac{-zIG_y}{y_i^2 + z^2} \right]^2 \tag{15}$$

where

y_i values of lateral displacement at which voltage measurements were made, ft

V_{y_i} voltage measurements of the y-channel output at y_i, volts

To find the value of the gain G_y, take the derivative of E with respect to G_y and set the result equal to zero.

$$\frac{dE}{dG_y} = \sum_i 2 \left(V_{y_i} + \frac{zIG_y}{y_i^2 + z^2} \right) \left(\frac{zI}{y_i^2 + z^2} \right) = 0 \tag{16}$$

An estimate of the gain is then

$$\hat{G}_y = - \frac{\sum_i \frac{zIV_{y_i}}{y_i^2 + z^2}}{\sum_i \left(\frac{zI}{y_i^2 + z^2} \right)^2} \tag{17}$$

With this value for the gain, the theoretical voltage V_y was computed as a function of y by using equation (5b), and the resulting curve is plotted in figure 9(a) along with the measured data V_{y_i}. Excellent agreement is obtained between the theoretical curve and the measurements in this case. This procedure was repeated for the other three filters, and the results are shown in figures 9(b) through 9(d). The theoretical and experimental results agree closely for the high-Q filters, but there is less agreement at the larger displacements when using the 990-Hz low-Q filter as shown in figure 9(c). Examination of the y-channel ac signal with an oscilloscope revealed the presence of interference believed to be a harmonic of the 400-Hz aircraft power. At displacements greater than about 20 ft the magnitude of this interference was larger than the desired signal.

Beginning with equation (5c), this procedure was repeated to find estimates of the other gains G_z and G_{zs} for each of the four filters. The resulting theoretical curves for V_{zs} are plotted in figure 10 together with the measured data. Once again good agreement is obtained between the theoretical and experimental data except for the case of the 990-Hz low-Q filter shown in figure 10(c). As before, the problem is interference, probably from the 400-Hz power. Similar good agreement was found for V_z.

Since the aircraft was assumed to be parallel to the cable, the theoretical voltage V_x would have been zero according to equations (5a) and (11a). However, some nonzero values for V_x and V_{xs} were measured at various displacements. This difference between theory and experiment was believed to be due to distortion of the magnetic field by the metal aircraft and by some small, but nonzero, heading Ψ. Without an accurate measurement of Ψ, good estimates of the gains G_x and G_{xs} could not be obtained with the above procedure. Therefore, in subsequent calculations the values of G_z and G_{zs} were used for G_x and G_{xs}, respectively.

As a measure of the quality of the signals at each frequency and bandwidth as a function of displacement from the cable, each of the 30-sec blocks of data recorded on magnetic tape was processed to determine the standard deviations of the output voltages for each filter. These results are plotted in figure 11 for V_y, V_z, and V_{zs}. Examination of the plots reveals that the standard deviations of V_y and V_z are significantly larger for the 990-Hz low-Q filter than for the other filters because of the interfering signal. The standard deviations of the 990-Hz high-Q filter output voltages appear to be slightly larger than those for the 150-Hz filters. The resulting signal-to-noise ratios for V_y are very good near the cable, with values in excess of 50 dB, and although they decrease with lateral displacement as expected, they appear adequate even at $y = 50$ ft, with values on the order of 25 to 30 dB. Signal-to-noise ratios for V_z are also good with peak values greater than 50 dB.

Displacement estimates. The tape recorded data were processed with equation (6) to compute time histories of the estimates $\hat{y}_1$ and $\hat{y}_{1s}$ of the lateral displacement for each block of data. In computing $\hat{y}_1$, measured values of V_y and V_z were used together with previously computed gain estimates $\hat{G}_y$ and $\hat{G}_z$. Because of the diode detector in the z-channel, the sign of V_z is always negative, so the sign of V_{zs} was used to determine the sign of $\hat{y}_1$. In computing $\hat{y}_{1s}$, measured values of V_y and V_{zs} were used in equation (6) together with gain estimates $\hat{G}_y$ and $\hat{G}_{zs}$. For each block of recorded data, the mean and standard deviation of $\hat{y}_1$ was calculated for each filter together with the error in the mean (mean of $\hat{y}_1 - y$). The resulting statistics are plotted in figure 12 for $\hat{y}_1$ and in figure 13 for $\hat{y}_{1s}$. Note in figure 12(b) that the error for the 990-Hz low-Q filter would be off scale and is not shown. A similar procedure was used to calculate time histories of the displacement estimates $\hat{y}_2$ and $\hat{y}_{2s}$ from equation (10). For each block of data the mean value, mean error, and standard deviation of the estimates were computed, and the results are plotted in figures 14 and 15 for $\hat{y}_2$ and $\hat{y}_{2s}$, respectively. As a typical example, time histories of the recorded data and of the computed estimates are plotted in figure 16 for the case of the 150-Hz high-Q filter with the aircraft at $y = 25$ ft.

The following observations are based on analysis of the static data voltage measurements and displacement estimates (figs. 9 through 15):

1. The mean errors in the displacement estimates obtained with the 990-Hz low-Q filter are sufficiently large to make that filter unusable, and subsequent observations will be directed toward the other three filters only. These large errors were caused by EMI from a harmonic of the 400-Hz aircraft power.
2. The mean errors and the standard deviations are smallest near the cable, where the best accuracy is desired.
3. At $y = 50$ ft, the mean errors in $\hat{y}_{1s}$ and $\hat{y}_{2s}$ are quite large.
4. The mean errors in $\hat{y}_1$ and $\hat{y}_2$ are comparable except in the case of the 990-Hz high-Q filter at $y = 50$ ft.
5. At 150 Hz the standard deviations of $\hat{y}_2$ are a little smaller than those for $\hat{y}_1$.
6. Both $\hat{y}_1$ and $\hat{y}_2$ are adequate for moderately accurate measurement of aircraft displacement, and both are preferred over $\hat{y}_{1s}$ and $\hat{y}_{2s}$. Differences between the estimates of $\hat{y}_2$ and $\hat{y}_1$ are small.
7. The system performed better at 150 Hz than at 990 Hz.
8. Performance of the high-Q and the low-Q filters at 150 Hz was similar.

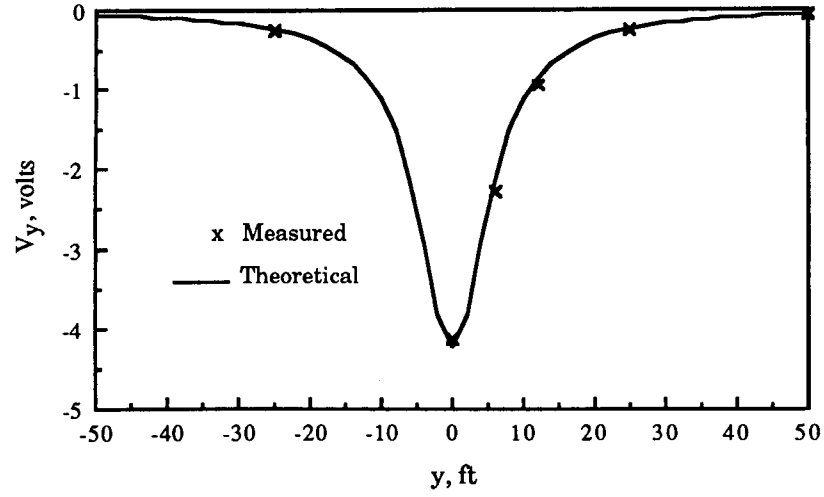

(a) 150-Hz low-Q filter.

Figure 9. Measured and theoretical y-channel output voltage.

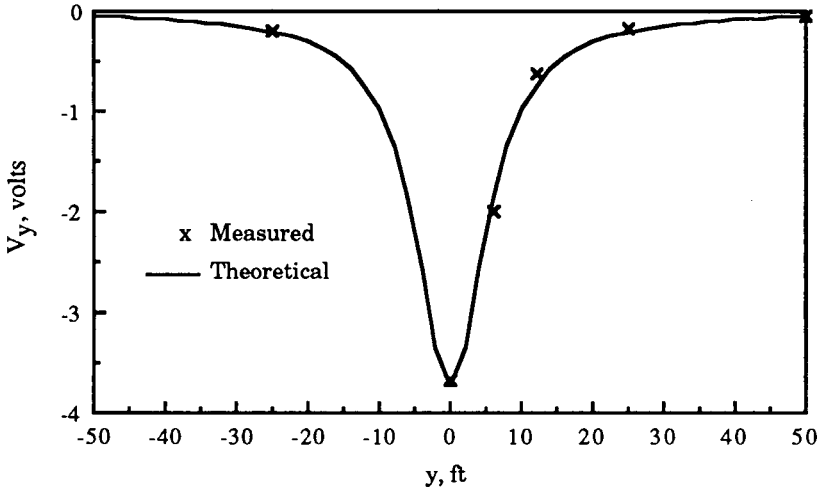

(b) 150-Hz high-Q filter.

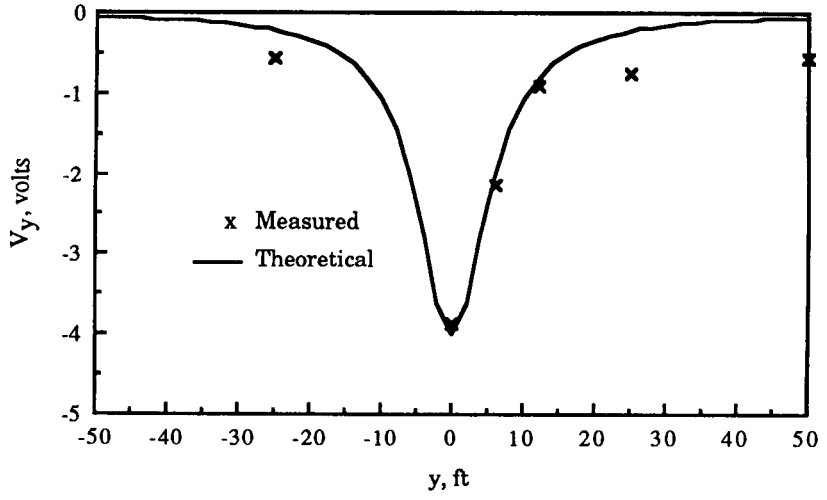

(c) 990-Hz low-Q filter.

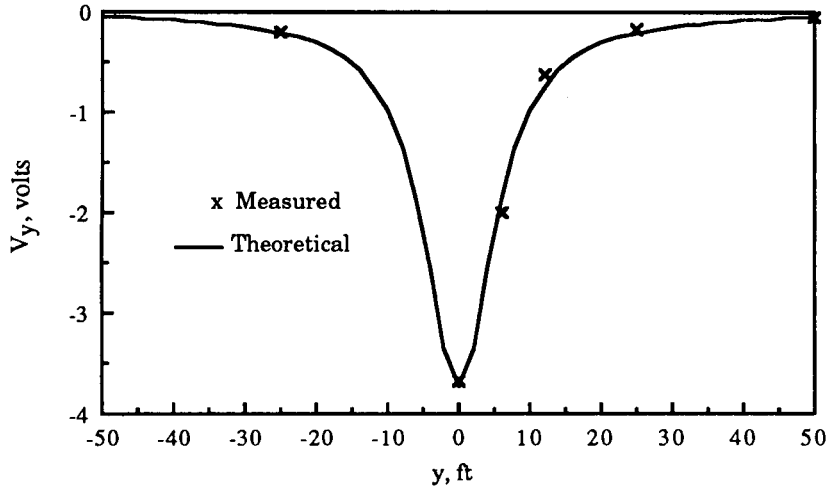

(d) 990-Hz high-Q filter.

Figure 9. Concluded.

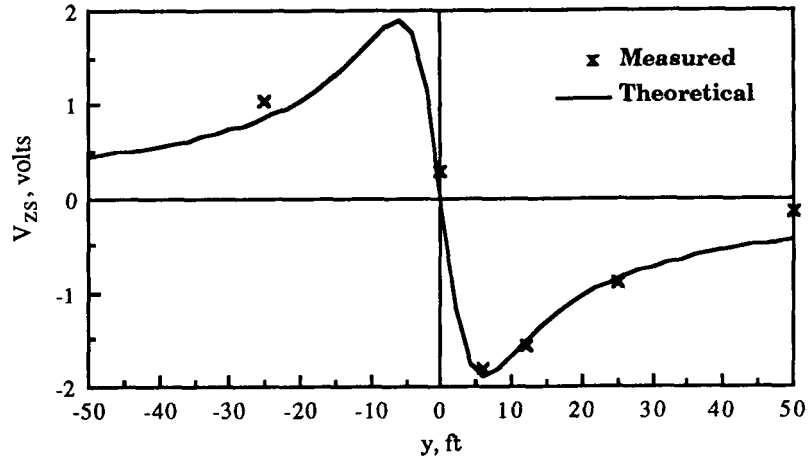

(a) 150-Hz low-Q filter.

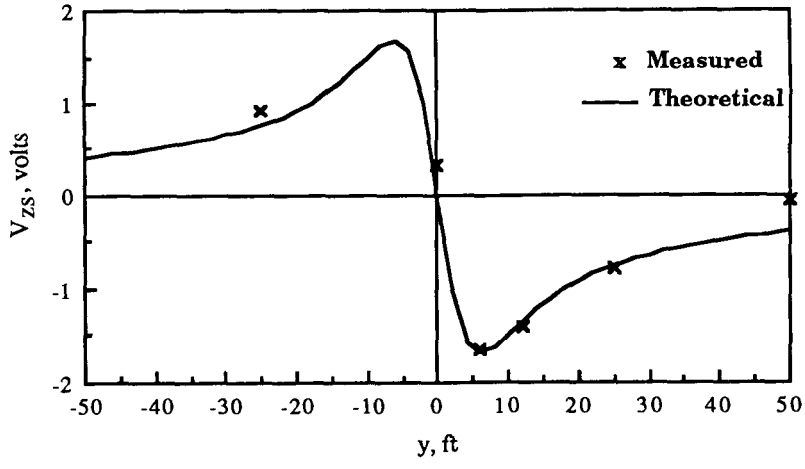

(b) 150-Hz high-Q filter.

Figure 10. Measured and theoretical zs-channel output.

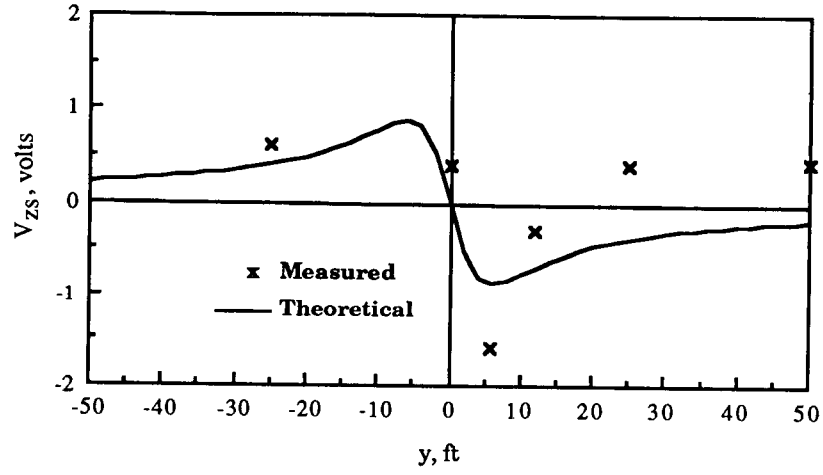

(c) 990-Hz low-Q filter.

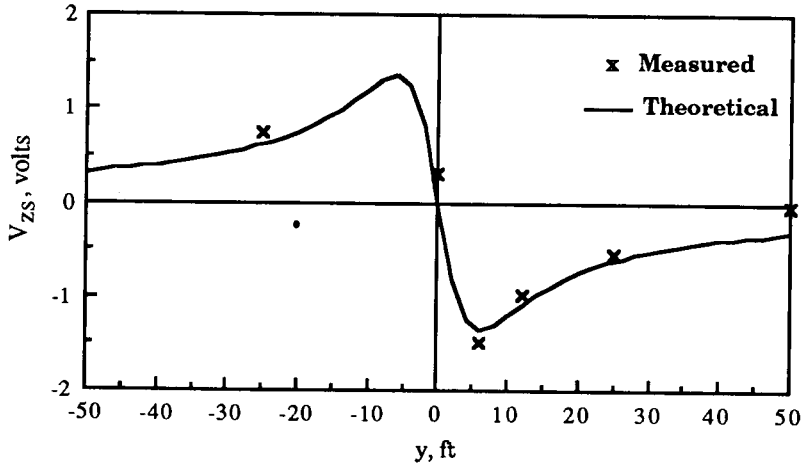

(d) 990-Hz high-Q filter.

Figure 10. Concluded.

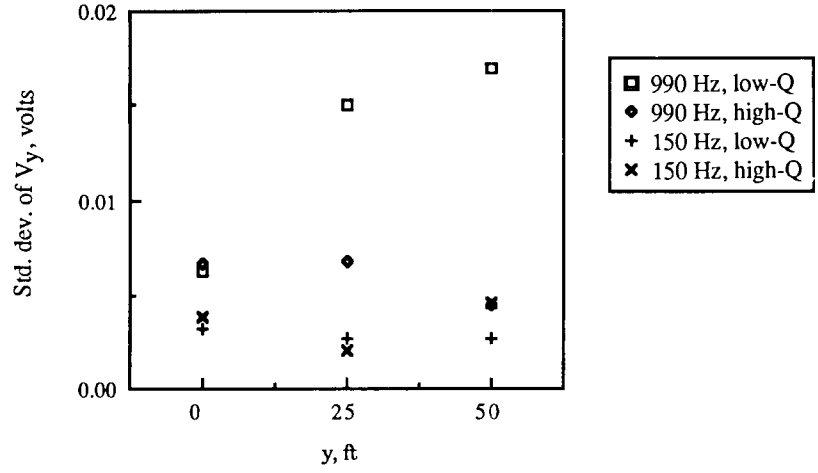

(a) y-channel.

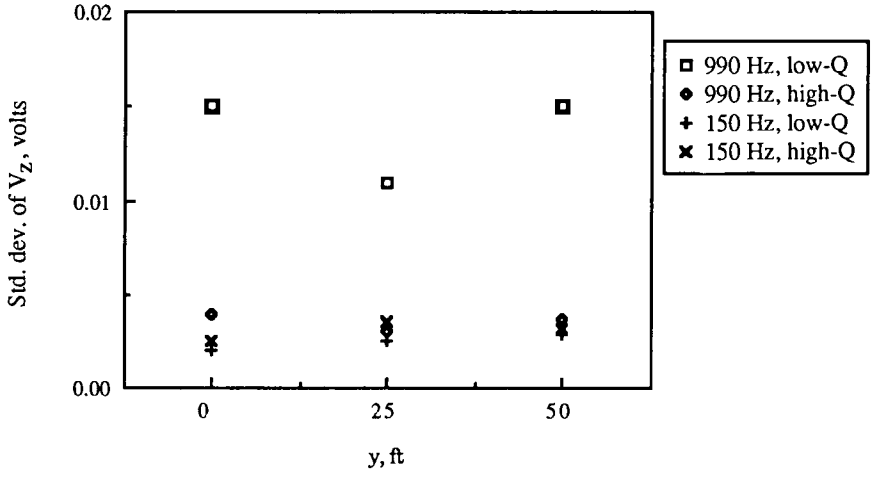

(b) z-channel.

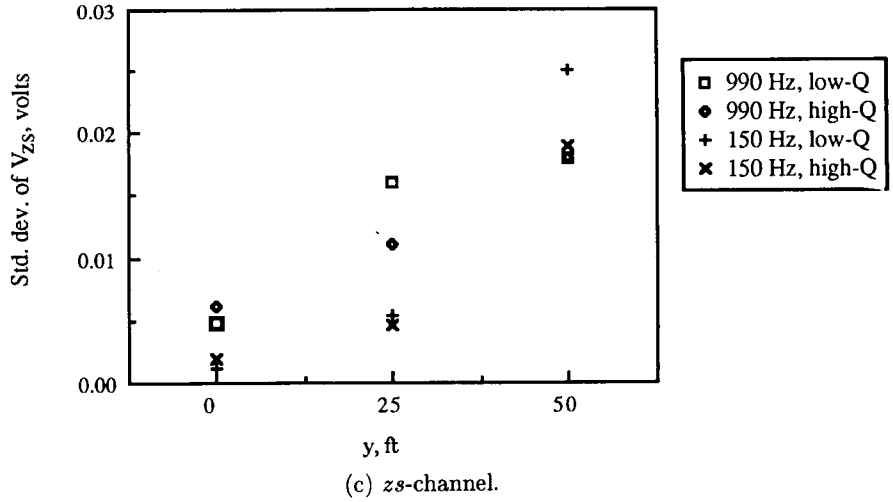

(c) zs-channel.

Figure 11. Standard deviation of the analog chassis output voltages.

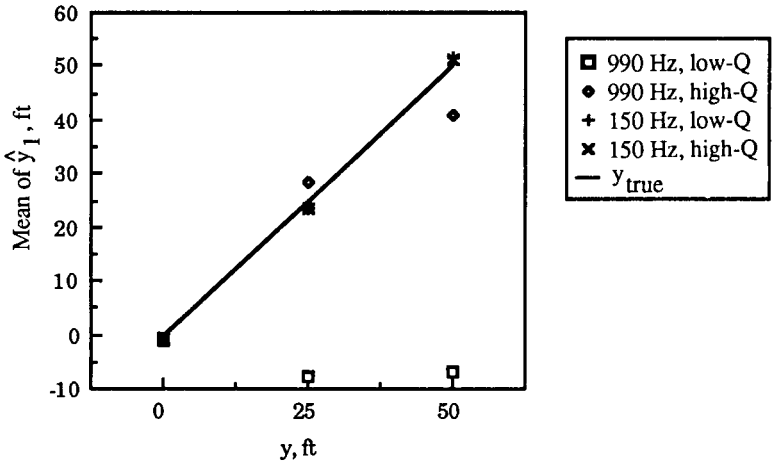

(a) Mean.

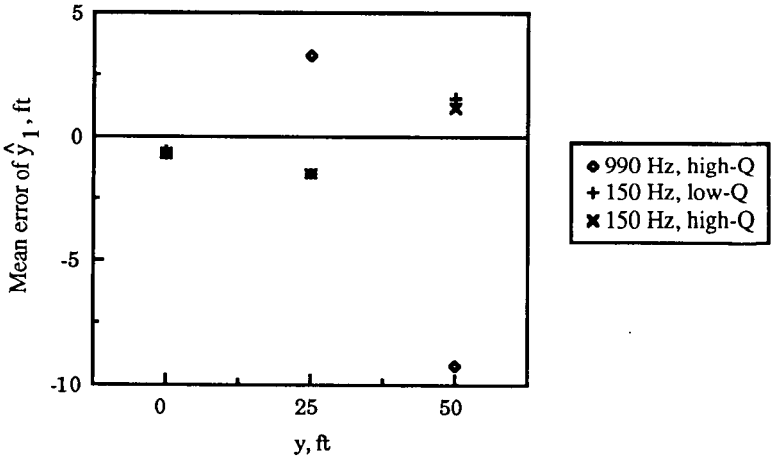

(b) Mean error.

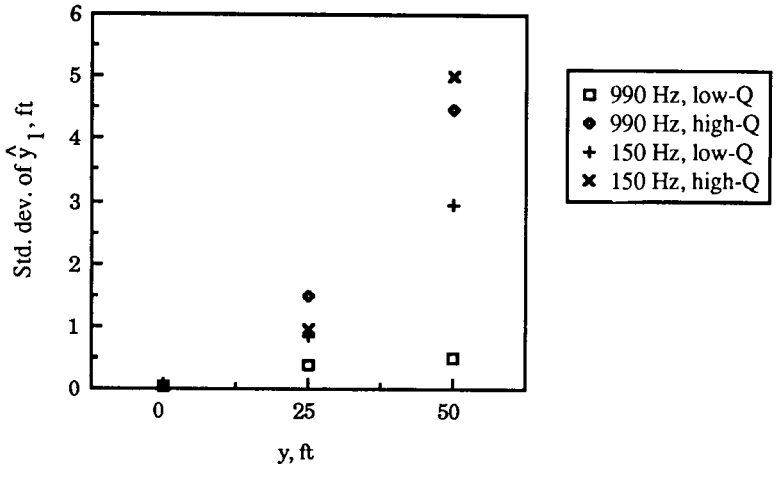

(c) Standard deviation.

Figure 12. Statistics of displacement estimate $\hat{y}_1$.

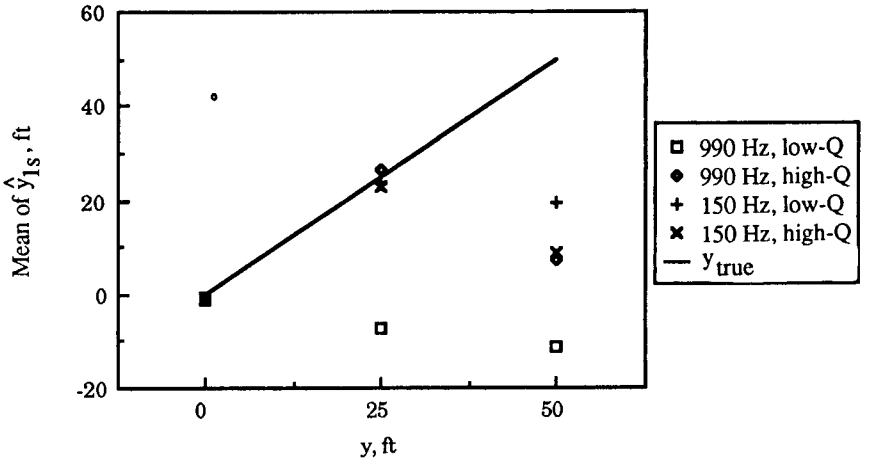

(a) Mean.

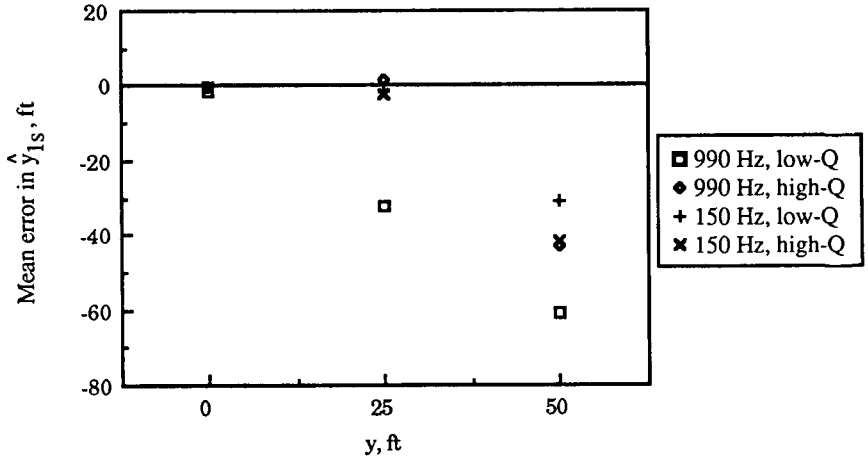

(b) Mean error.

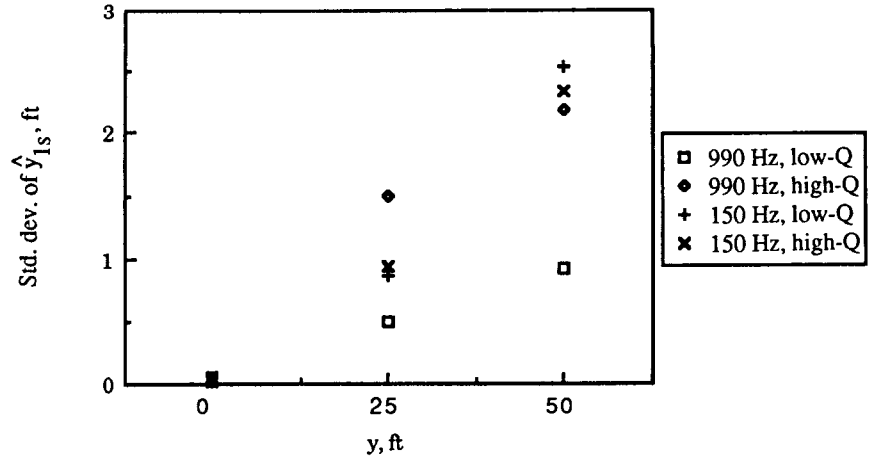

(c) Standard deviation.

Figure 13. Statistics of displacement estimate $\hat{y}_{1s}$.

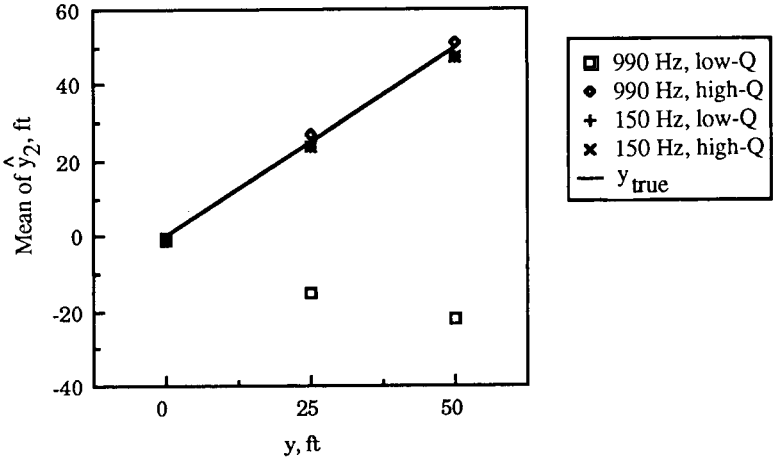

(a) Mean.

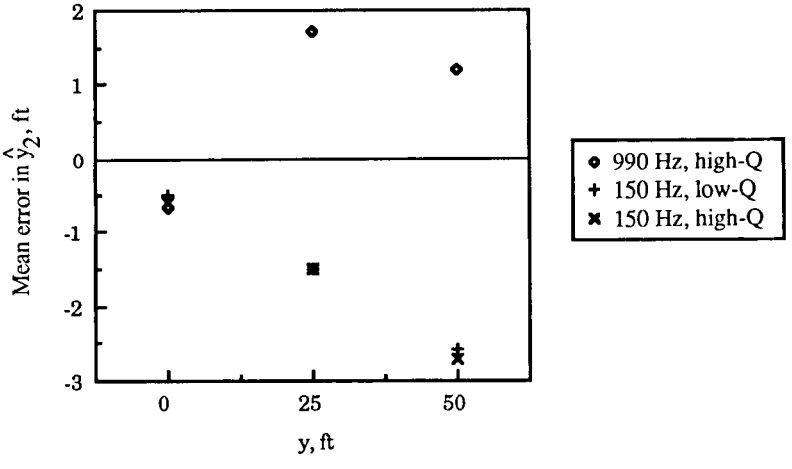

(b) Mean error.

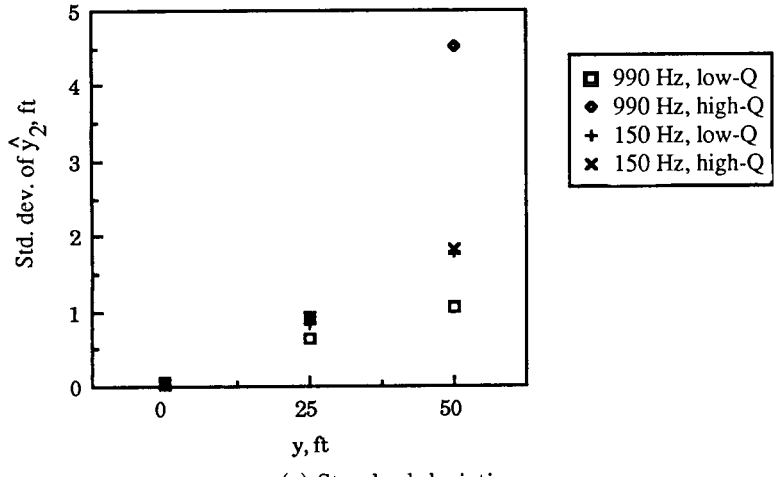

(c) Standard deviation.

Figure 14. Statistics of displacement estimate $\hat{y}_2$.

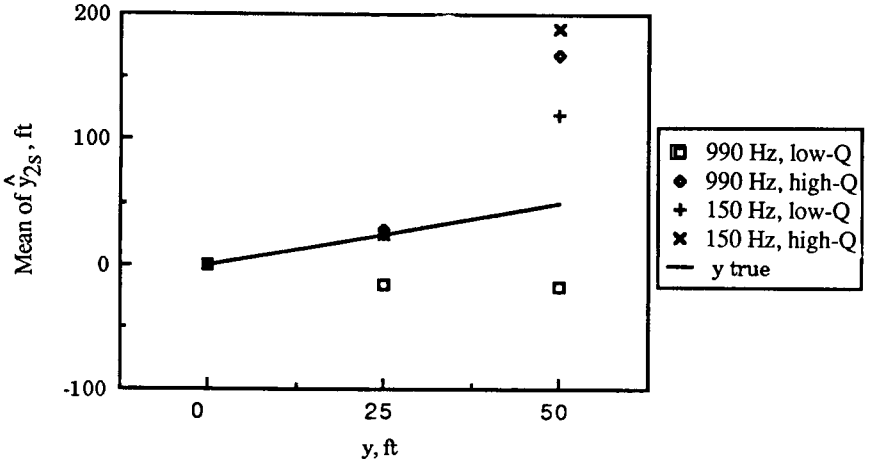

(a) Mean.

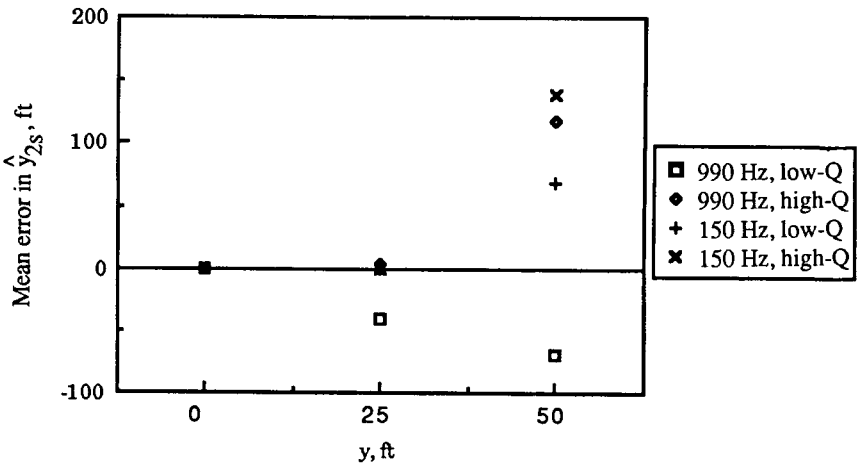

(b) Mean error.

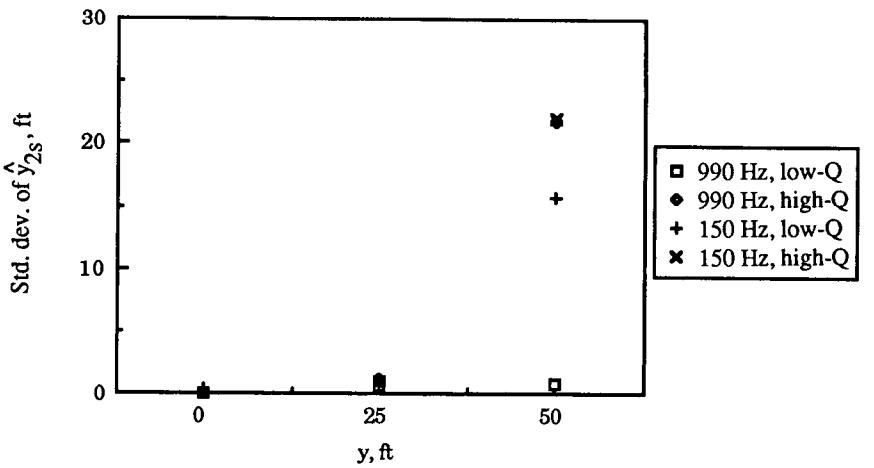

(c) Standard deviation.

Figure 15. Statistics of displacement estimate $\hat{y}_{2s}$.

Heading estimate. In a similar manner, the tape recorded measurements of V_y and V_x together with gain estimates $\hat{G}_y$ and $\hat{G}_x$ were processed with equation (13) to compute time histories of the estimates $\hat{\Psi}$ of relative heading for each block of data. Recall that an independent estimate $\hat{G}_x$ of the gain in the x-channel was not computed, but that $\hat{G}_x$ was set equal to $\hat{G}_z$. Because of the diode detector in the x-channel, the sign of V_x is always negative, so the sign of $\hat{\Psi}$ was set equal to the sign of V_{xs} . For each block of data, the mean and standard deviation of $\hat{\Psi}$ were calculated for each filter. The resulting means are plotted in figure 17.

From figure 17(a) it can be seen that the heading estimates obtained with the 990-Hz filters were grossly in error. The estimates obtained with the 150-Hz filters are also inaccurate except near centerline and vary almost linearly with displacement y, as can be seen on an expanded scale in figure 17(b). Therefore, with any of the filters, the heading estimates appear to be unusable. The large errors are believed to be caused by distortion of the magnetic field by the metal aircraft, which seems to produce an x-component of the field even when the aircraft heading is zero (except, perhaps, when the aircraft is on centerline).

Dynamic Tests

A series of dynamic tests were conducted in which the aircraft was taxied down the runway, onto the high-speed turnoff, and then along the taxiway under manual pilot control at a speed of around 20 knots while data (the analog chassis dc output voltages V_x, V_{xs}, V_y, V_z, and V_{zs}) were recorded on magnetic tape. The duration of each of these runs was on the order of 5 min. The purpose of these tests was to evaluate signal quality and MLC system performance in terms of the quality of the displacement and heading estimates as a function of position along the runway, turnoff, and taxiway. Also of interest were degradation in performance during the turns, transients caused by transition from one runway construction material to another, periodic effects such as might be produced by reinforcement in the concrete, and power line interference. Analysis of the data was more qualitative than quantitative because dynamic ground truth data (true values of aircraft displacement and heading) of even moderate accuracy were not available.

Three runs were made along the centerline ($y = 0$), one run each with the 990-Hz high-Q, 150-Hz low-Q, and 150-Hz high-Q filters. Time histories of the recorded data and the postflight computed estimates for the 150-Hz low-Q filter run are plotted in figure 18. Notice that the pilot was taxiing along a path parallel to and about 5 ft away from the centerline for the first 60 sec. Note that during this time the heading estimate $\hat{\Psi}$ exhibited a bias similar to that found in the static data (fig. 17(b)). There are several noise bursts or spikes in the output voltages and in the estimates during the first 40 sec of the run and during the last 40 sec. These anomalies were caused by EMI from the aircraft's VHF and UHF radio voice communications transmitters. It is believed that this interference can be reduced to a tolerable level with the proper filtering. Except for this EMI both estimates of displacement appear to be of high quality throughout the run, even during the turnoff, which occurred between 155 and 205 sec into the run.

Two more dynamic runs, one with the 150-Hz low-Q filter and one with the 150-Hz high-Q filter, were made with the pilot steering the aircraft in a sinusoidal pattern as he taxied down the runway, turnoff, and taxiway. Time history data for the 150-Hz high-Q filter run are shown in figure 19. The half-wave rectifying action of the diode detector is apparent in the V_y and V_z data, which are always negative. On the other hand, the V_{zs} data change sign as the aircraft crosses the centerline, thereby allowing the MLC system to determine whether the aircraft is to the right or left of center. Relatively noise-free estimates of displacement were obtained throughout the run with no significant differences between $\hat{y}_1$ and $\hat{y}_2$ noticeable in the plots. Note that the heading estimates were nearly in phase with the displacement estimates. Therefore, occurrences of the maximum magnitudes in $\hat{\Psi}$ nearly coincided with the maximum magnitudes of $\hat{y}_1$ and $\hat{y}_2$, whereas the true heading was zero at these points, and the points of maximum magnitude in heading occurred near centerline crossover. Again the effects of EMI from the radio transmitters were present early in the run. The data for the 150-Hz low-Q filter run were very similar to high-Q filter data in figure 19. The results of the dynamic runs indicate that the displacement estimates are usable, while the heading estimate is not.

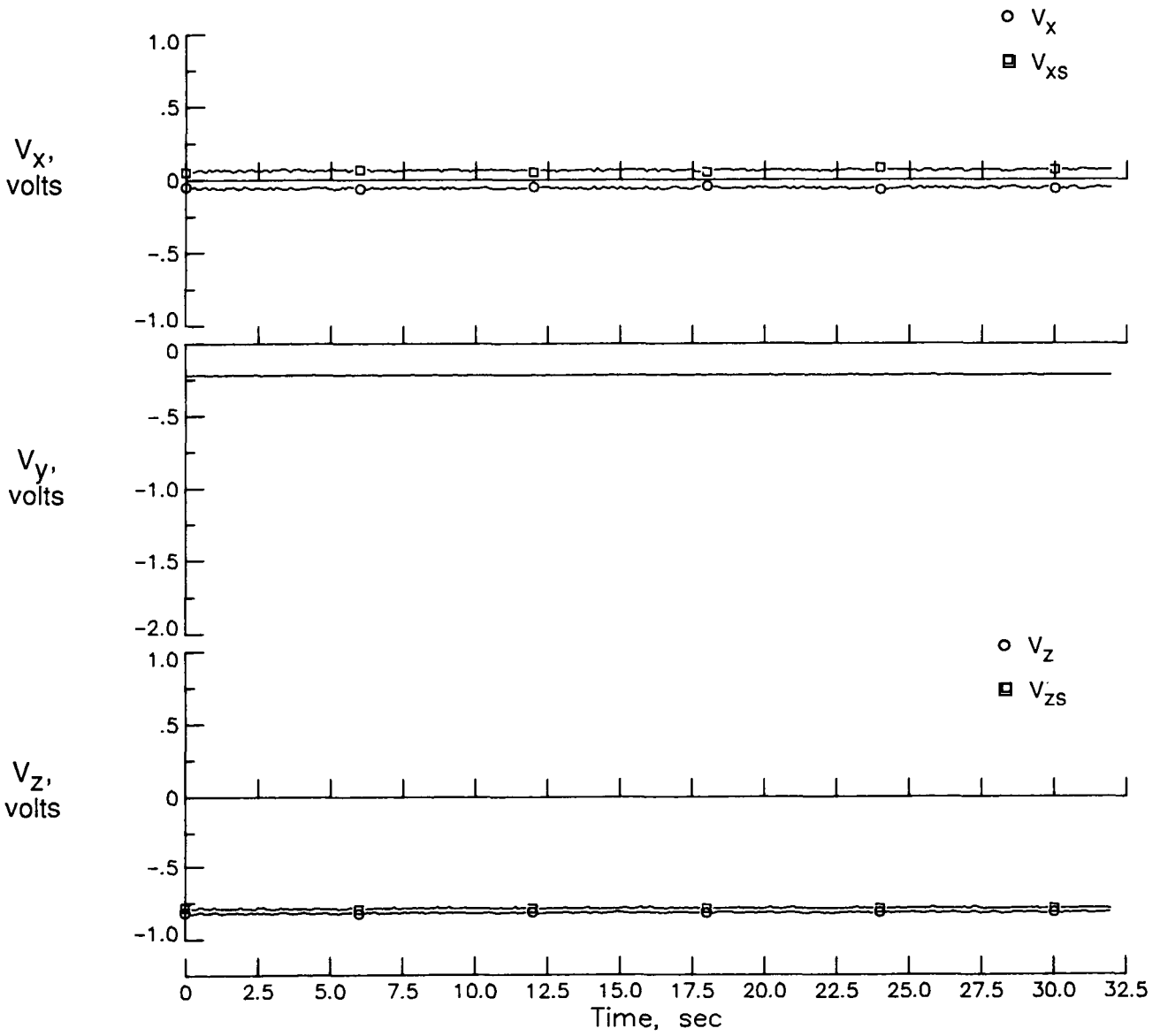

Figure 16. Typical time history output voltages and displacement estimates.

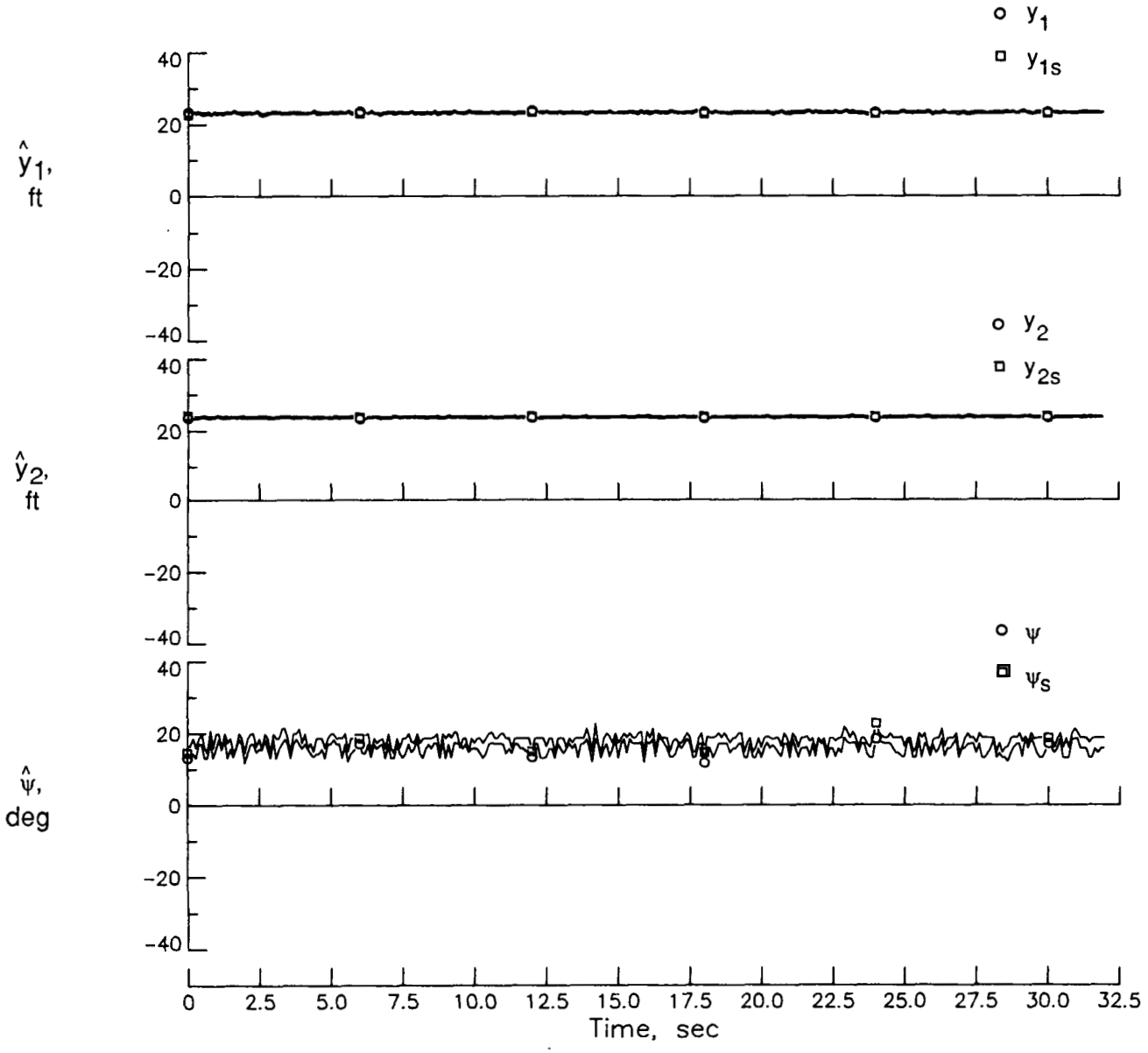

Figure 16. Concluded.

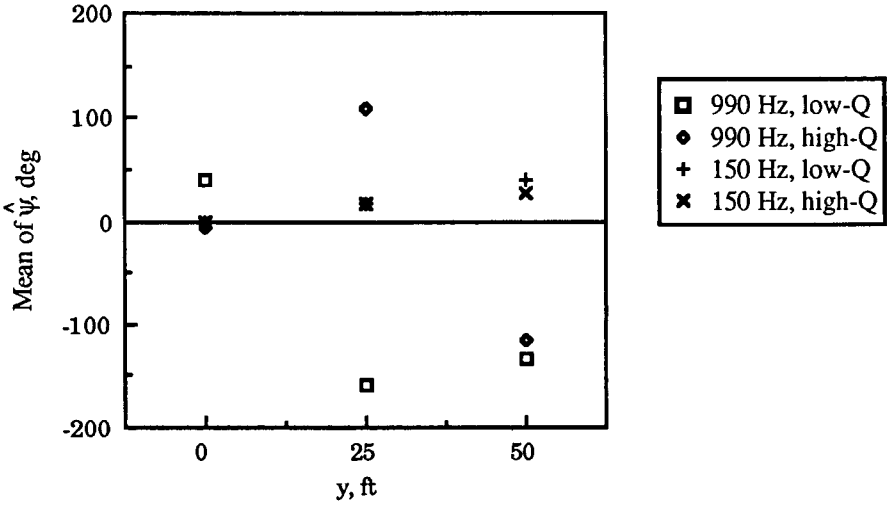

(a) Mean.

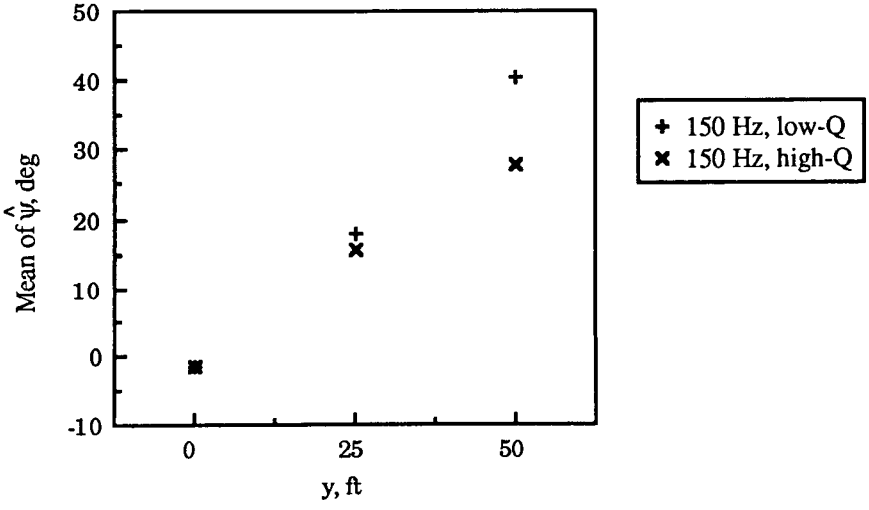

(b) Mean for 150-Hz filters only.

Figure 17. Mean values of estimate $\hat{\Psi}$.

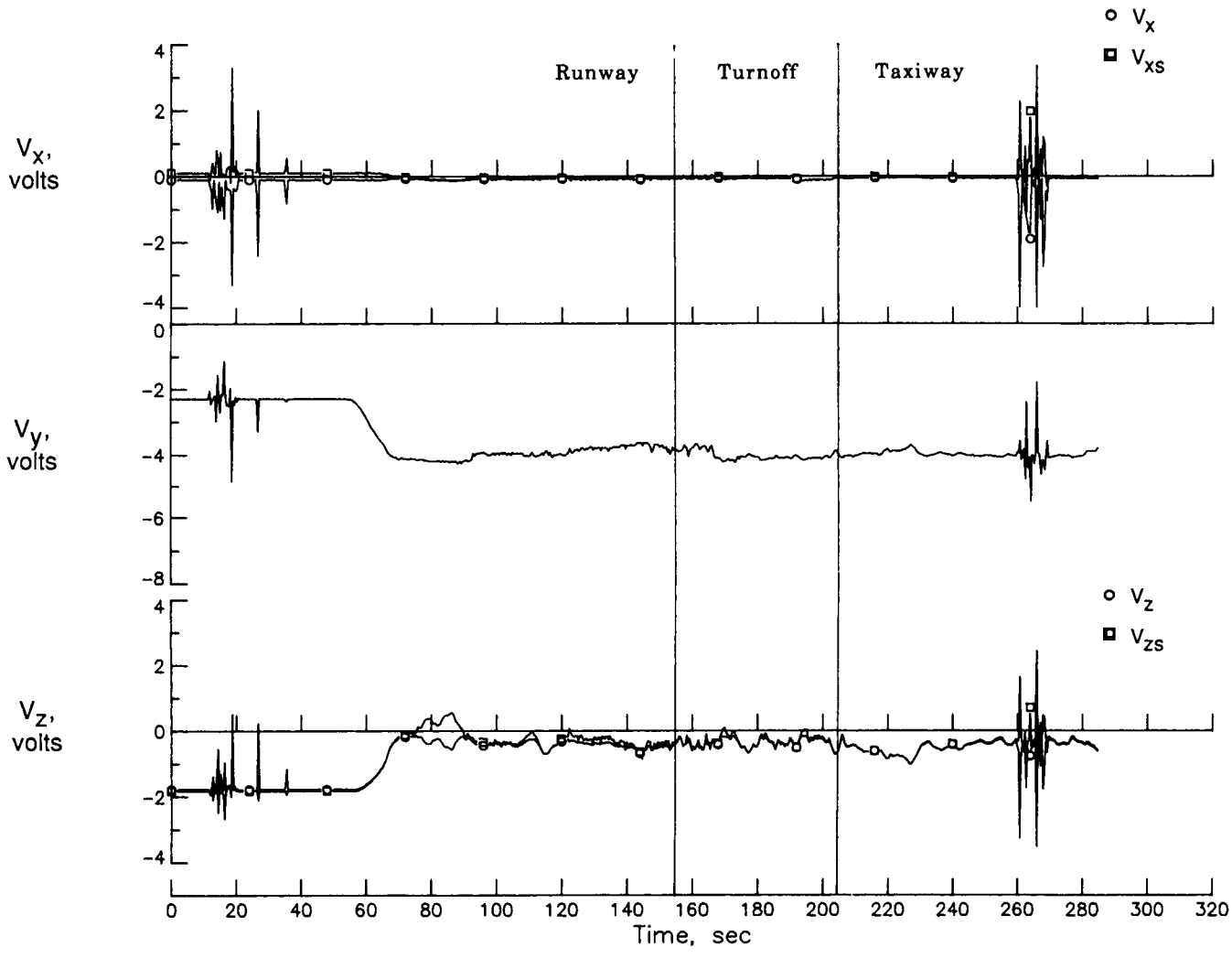

Figure 18. Time history of data for dynamic run along centerline. 150-Hz low-Q filter.

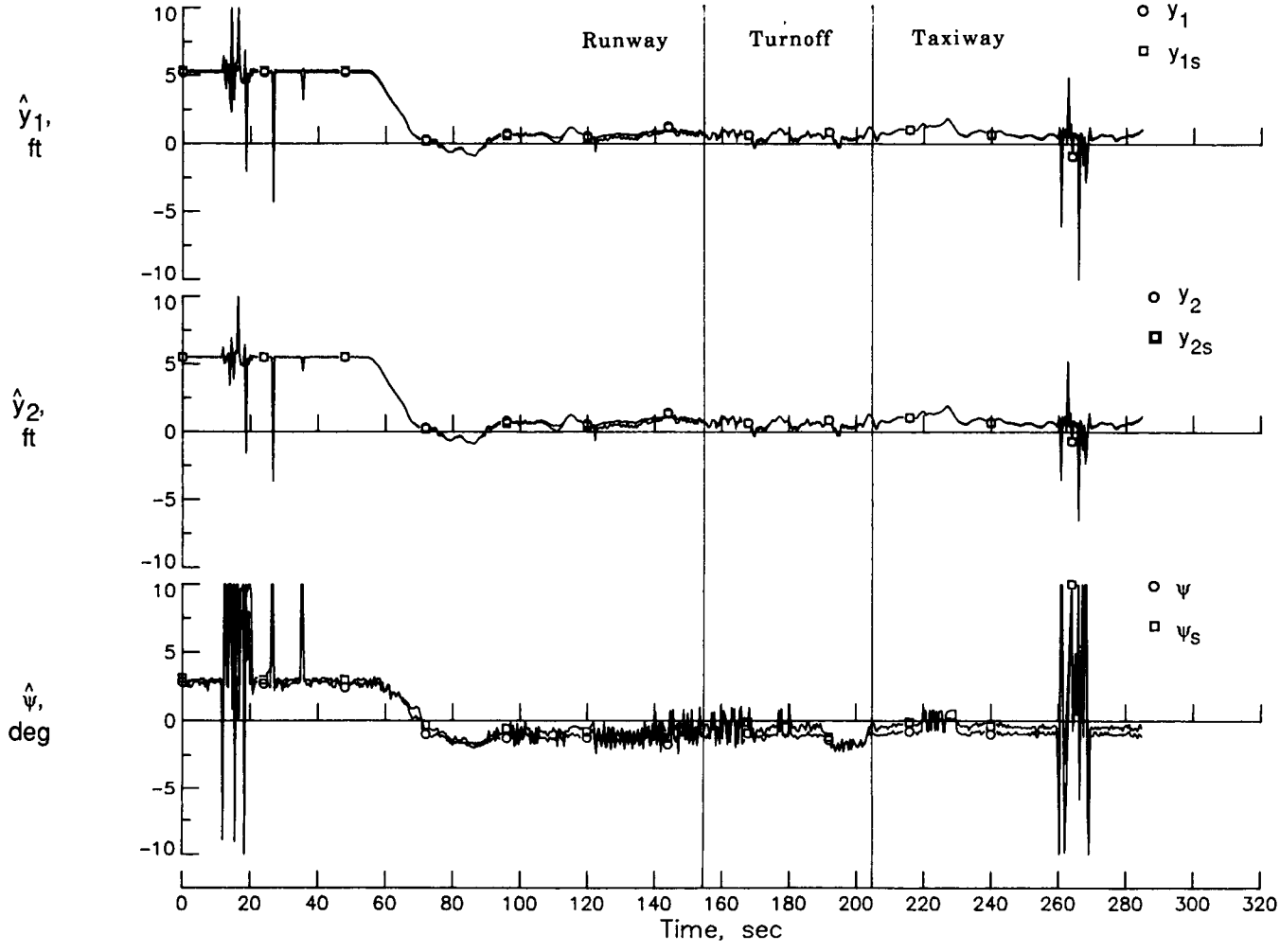

Figure 18. Concluded.

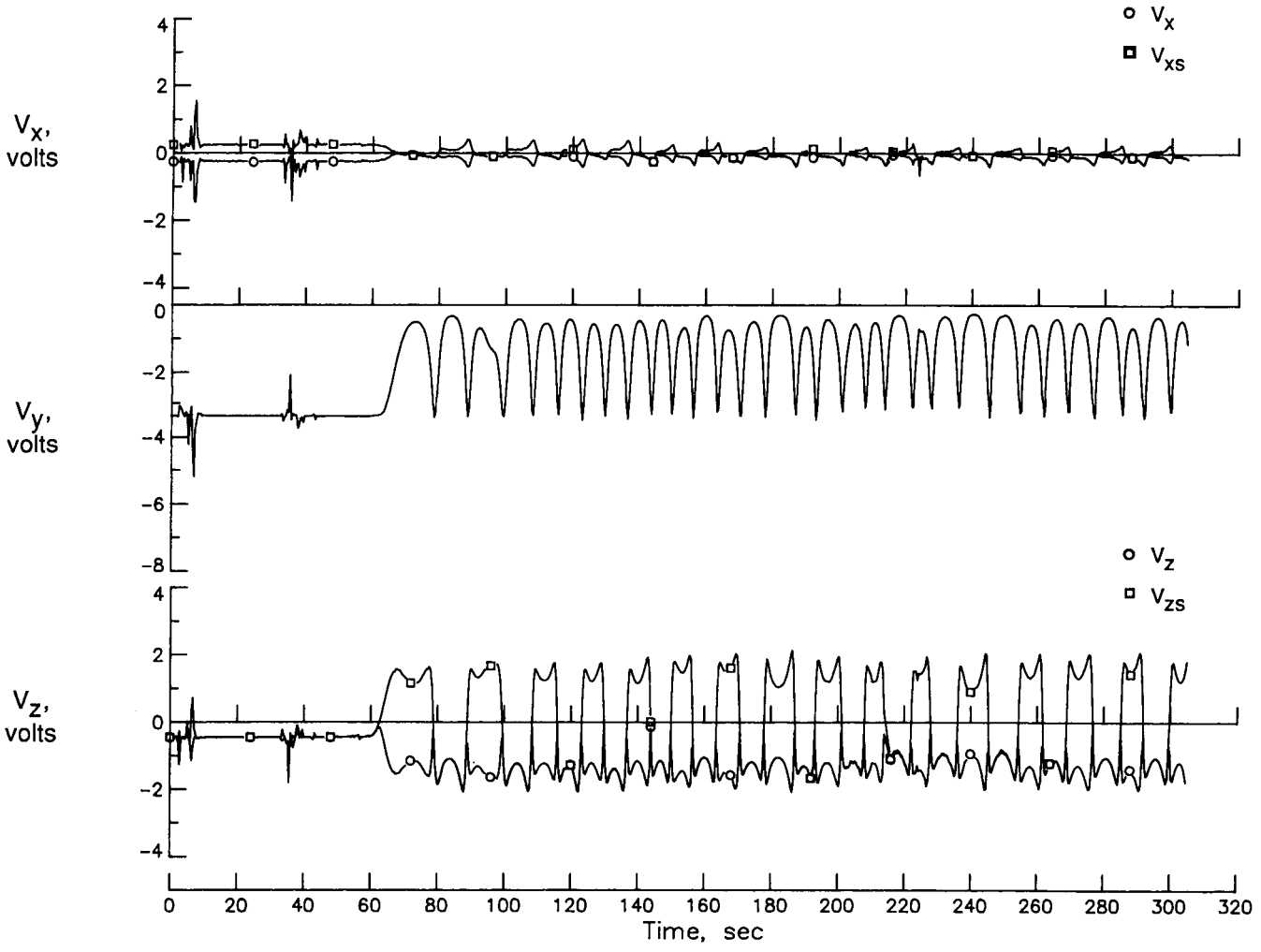

Figure 19. Time history of data for dynamic run along sinusoidal path about centerline. 150-Hz high-Q filter.

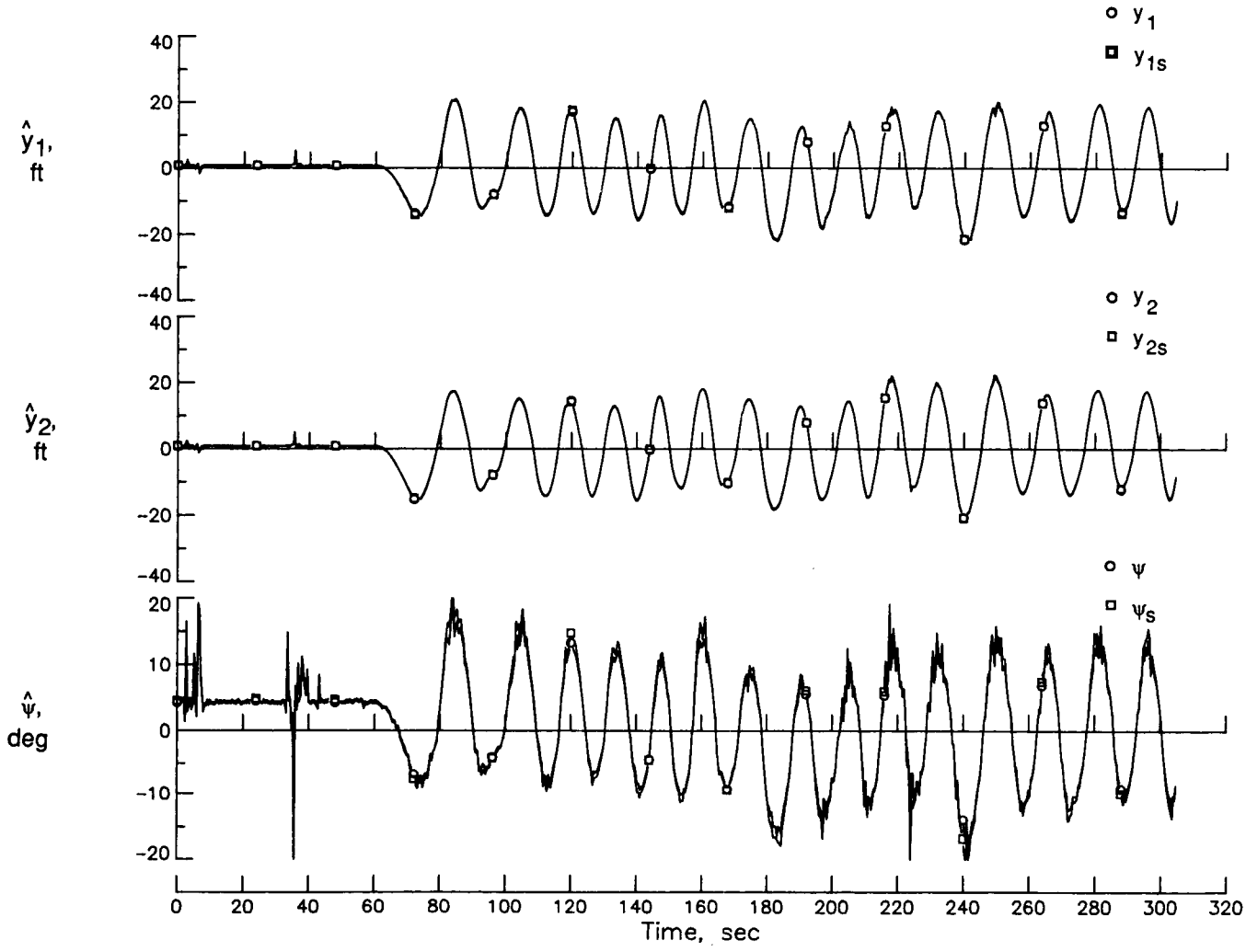

Figure 19. Concluded.

EMI Tests

Several additional tests were conducted to gather more information relative to the EMI appearing on the analog chassis outputs. While the aircraft was parked near centerline for the static tests at $y \approx 0$, data were recorded on the flight data system for approximately 100 sec for each of the filter/bandwidth combinations while the aircraft avionics systems were turned off one at a time and left off. Shown in figure 20 are time history plots of the analog chassis dc voltage outputs and of the displacement and heading estimates for the 990-Hz low-Q, wideband filter, which was the filter most severely affected by the aircraft ac power interference, as previously noted. Note the jumps in the levels of V_x and V_z as the various systems were switched off. The most noticeable jump occurred at approximately 110 seconds when the pitot heat was switched off. The magnitude of V_{xs} was much smaller than the magnitude of V_x because the interference was asynchronous with the MLC ac signal in the y-channel, which drives the synchronous detector. Note that even with the interference, the errors in the displacement estimates $\hat{y}_1$ and $\hat{y}_2$ were less than 2 ft. Similar data are plotted for the 150-Hz high-Q narrowband filter in figure 21. Notice the relative lack of noise on the signals and the absence of jumps when the various avionics were switched off, indicating that most of the interference has been filtered out. The displacement estimates $\hat{y}_1$, $\hat{y}_{1s}$, $\hat{y}_2$, and $\hat{y}_{2s}$ were nearly equal with errors of only about 0.6 ft.

After the static tests were conducted at $y \approx 25$ ft, additional EMI tests were performed at each filter/bandwidth combination by recording data on the flight data system while each of the communications transmitters were operated for several seconds. Time history plots of the analog chassis outputs and of the displacement and heading estimates for the 150-Hz high-Q filter are shown in figure 22. The VHF1, VHF2, and UHF transmitters were "keyed on" at approximately 38, 50, and 58 sec, respectively. For each output voltage the transmitter interference was much larger than the signal, and the accuracy of the displacement estimates was destroyed. How this interference entered into the MLC system is currently unknown and must be determined; however, it is anticipated that the interference can be suppressed with filtering. Note in figure 22 that when neither of the transmitters was being used, good estimates of the aircraft displacement were obtained.

Conclusions

An experimental magnetic leader cable (MLC) system designed to measure aircraft lateral displacement from and heading relative to centerline, and thus provide guidance information to the aircraft during roll-out, turnoff, and taxi, was tested at Wallops Flight Facility in NASA's Transport System Research Vehicle (TSRV), a modified Boeing 737. The experimental equipment operated at either of two frequencies (150 Hz and 990 Hz) and with one of two filters (low-Q wideband or high-Q narrowband) at either frequency. Static tests were conducted with the aircraft parked on the runway at various displacements from and approximately parallel to the cable. Dynamic tests were conducted with the pilot taxiing the aircraft under manual control along the runway, turnoff, and taxiway. In posttest processing, estimates of the lateral displacement (using two different algorithms) and of the relative heading were computed. Results of these tests indicate the following:

1. Electromagnetic interference (EMI) from the aircraft's 400-Hz power system makes the 990-Hz low-Q wideband filter unusable. This interference is reduced to a tolerable level when any of three other filters are used.

2. The estimate of relative heading was found to be a strong function of displacement from the cable and is not sufficiently accurate to be usable. The primary source of error is believed to be distortion of the magnetic field by the metal aircraft. The errors in the heading estimates were larger at 990 Hz than at 150 Hz. If heading is required during roll-out and turnoff, it must be obtained from other sources, such as an inertial navigation system.

3. The performance of the MLC system is degraded by EMI from the aircraft's VHF and UHF voice communication radio during periods of transmission, and further research on suppressing this interference is required.

4. The estimates ($\hat{y}_1$ and $\hat{y}_2$) of displacement computed with voltage magnitude from the diode detector and sign from the synchronous detector are superior to the estimates ($\hat{y}_{1s}$ and $\hat{y}_{2s}$) computed with magnitude and sign from the synchronous detectors.

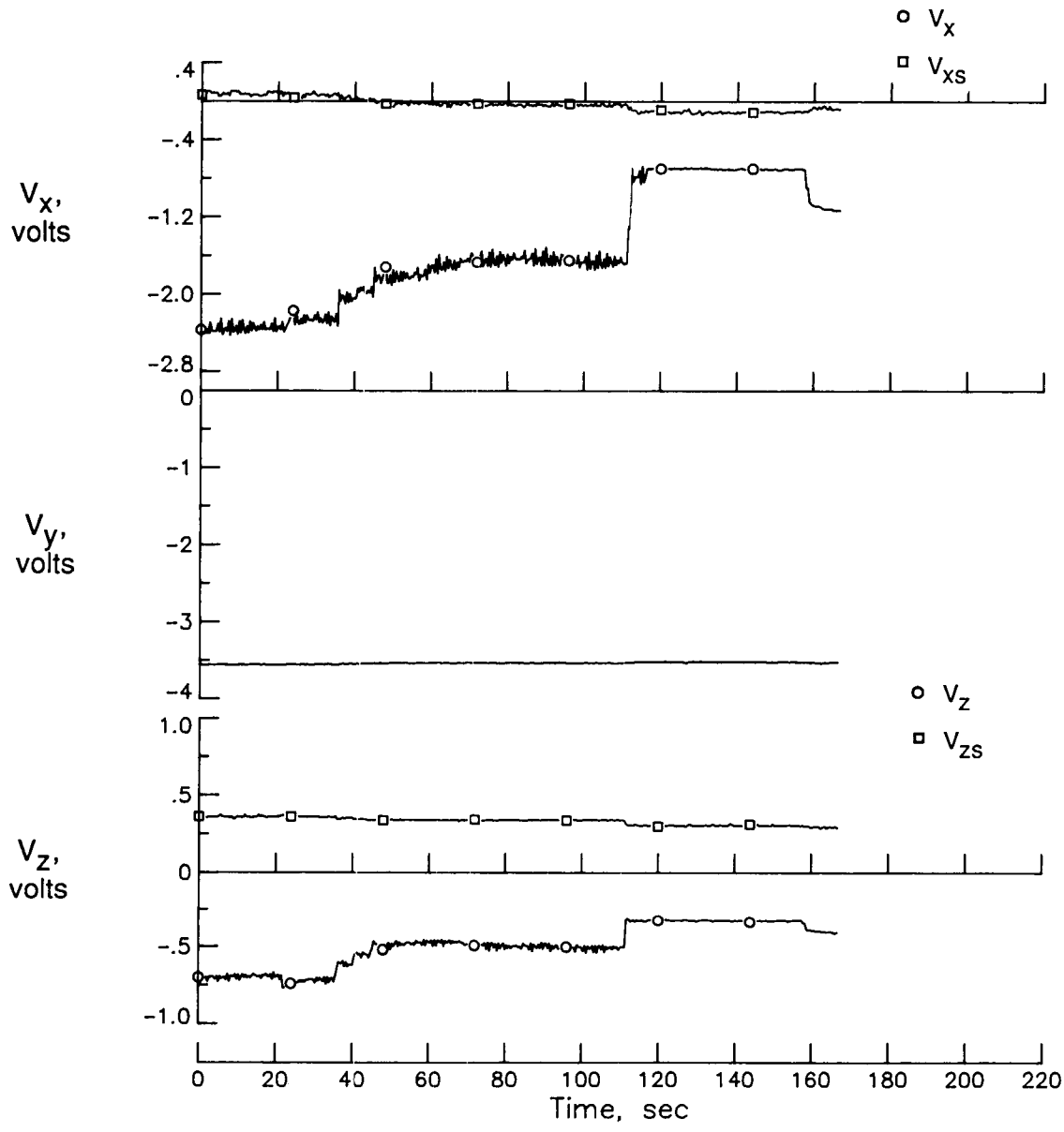

Figure 20. Time history of data for EMI test near centerline with 990-Hz low-Q filter showing interference from aircraft 400-Hz power.

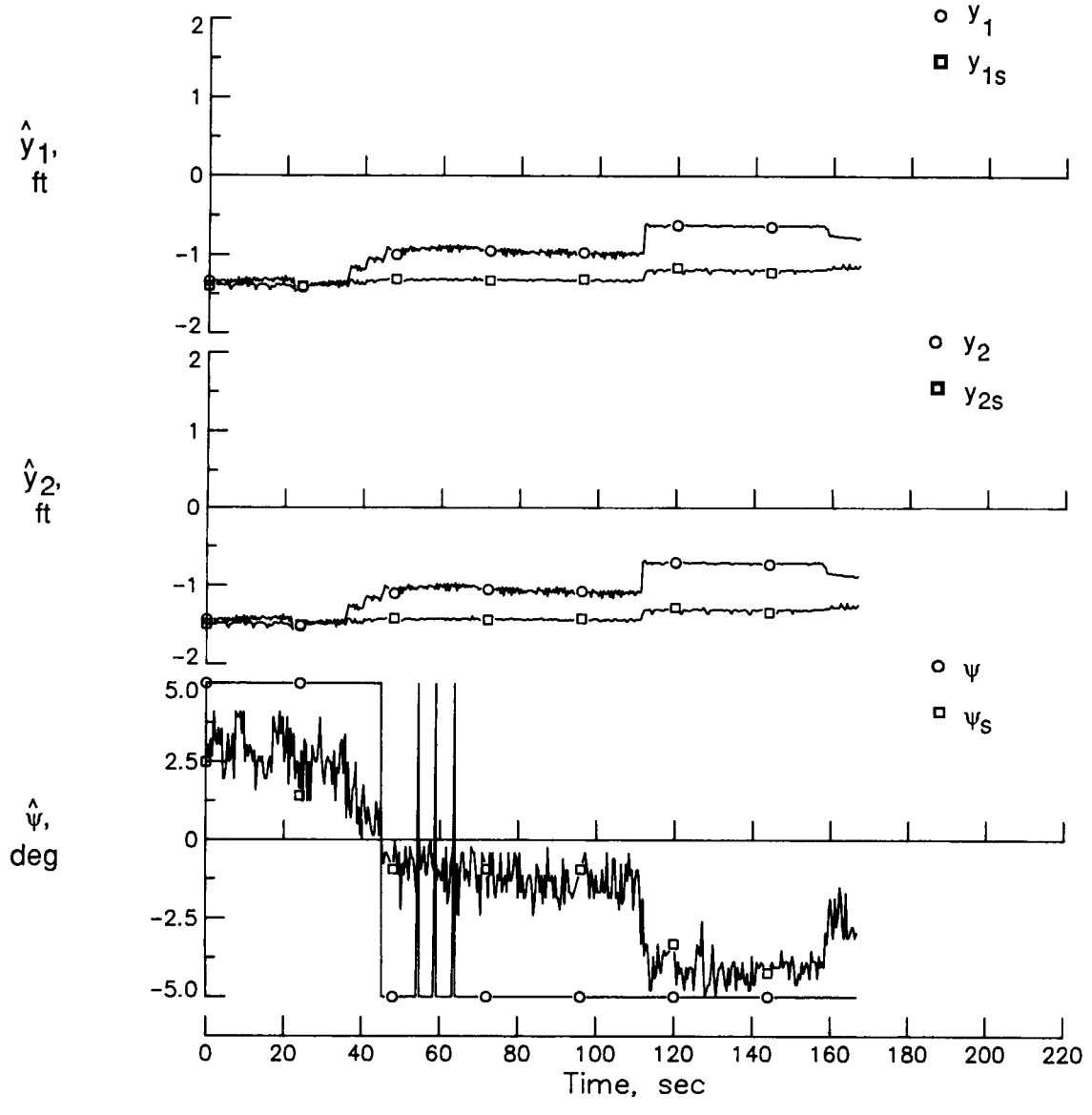

Figure 20. Concluded.

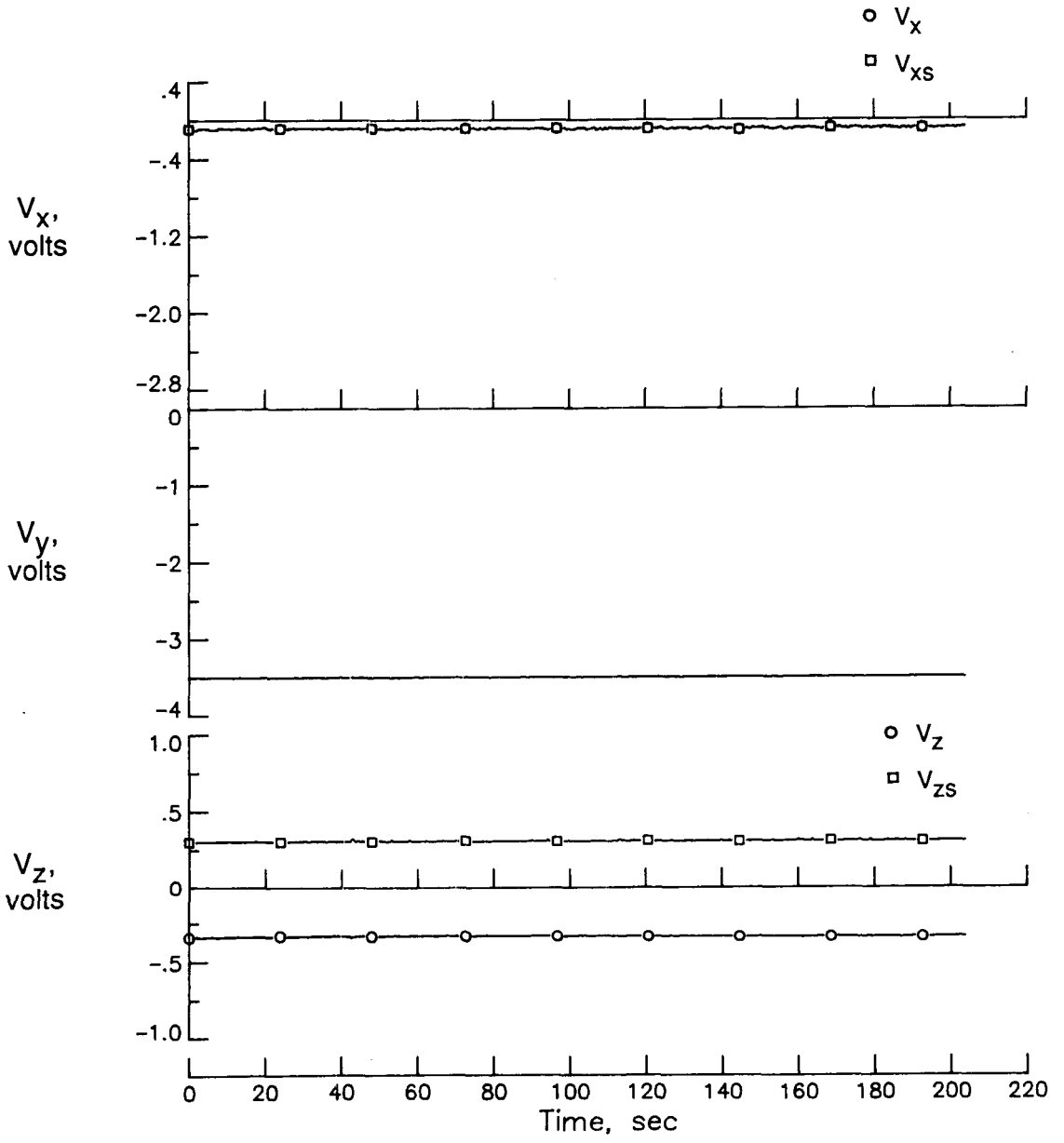

Figure 21. Time history of data for EMI test near centerline with 150-Hz high-Q filter.

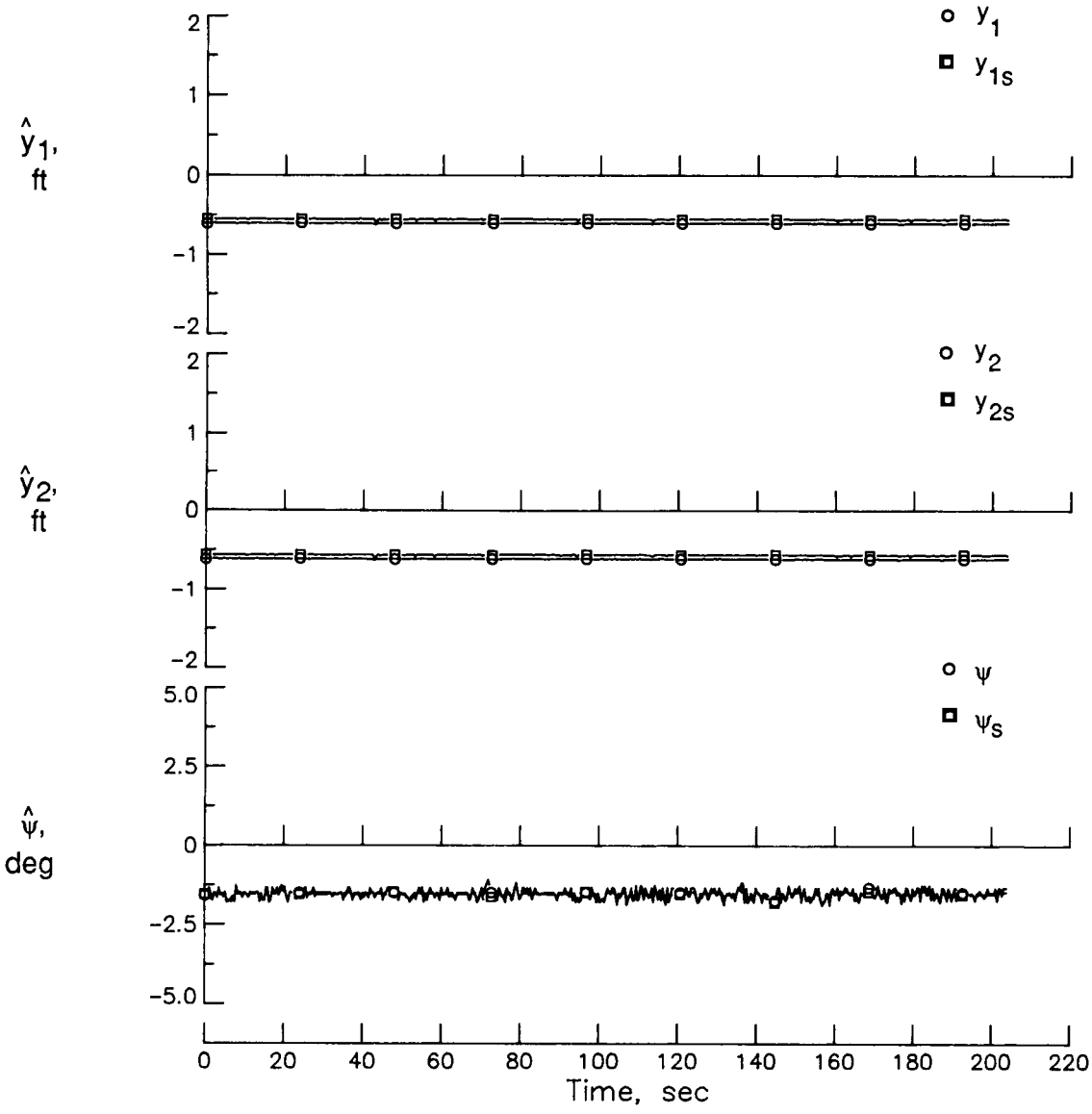

Figure 21. Concluded.

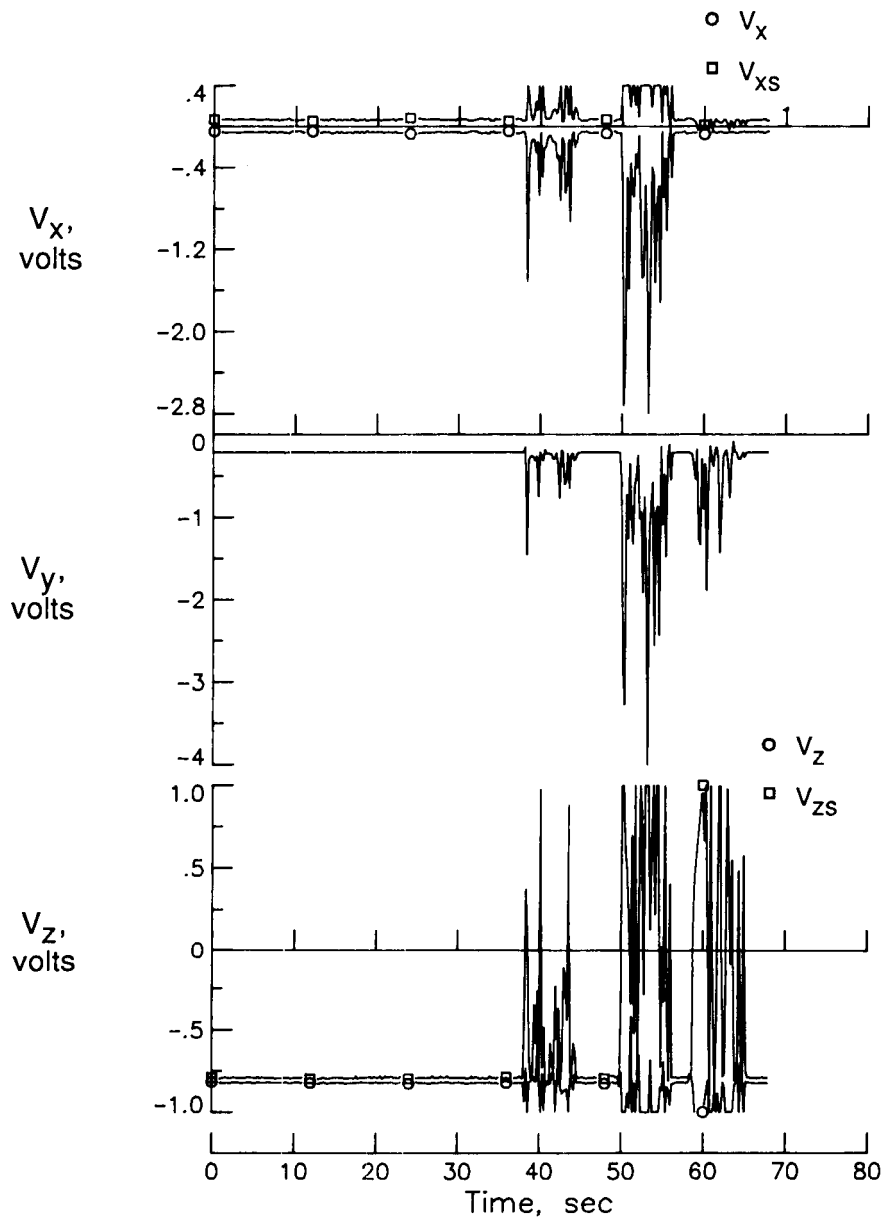

Figure 22. Time history of data for EMI test at $y \approx 25$ ft with 150-Hz high-Q filter showing interference from communications transmitters.

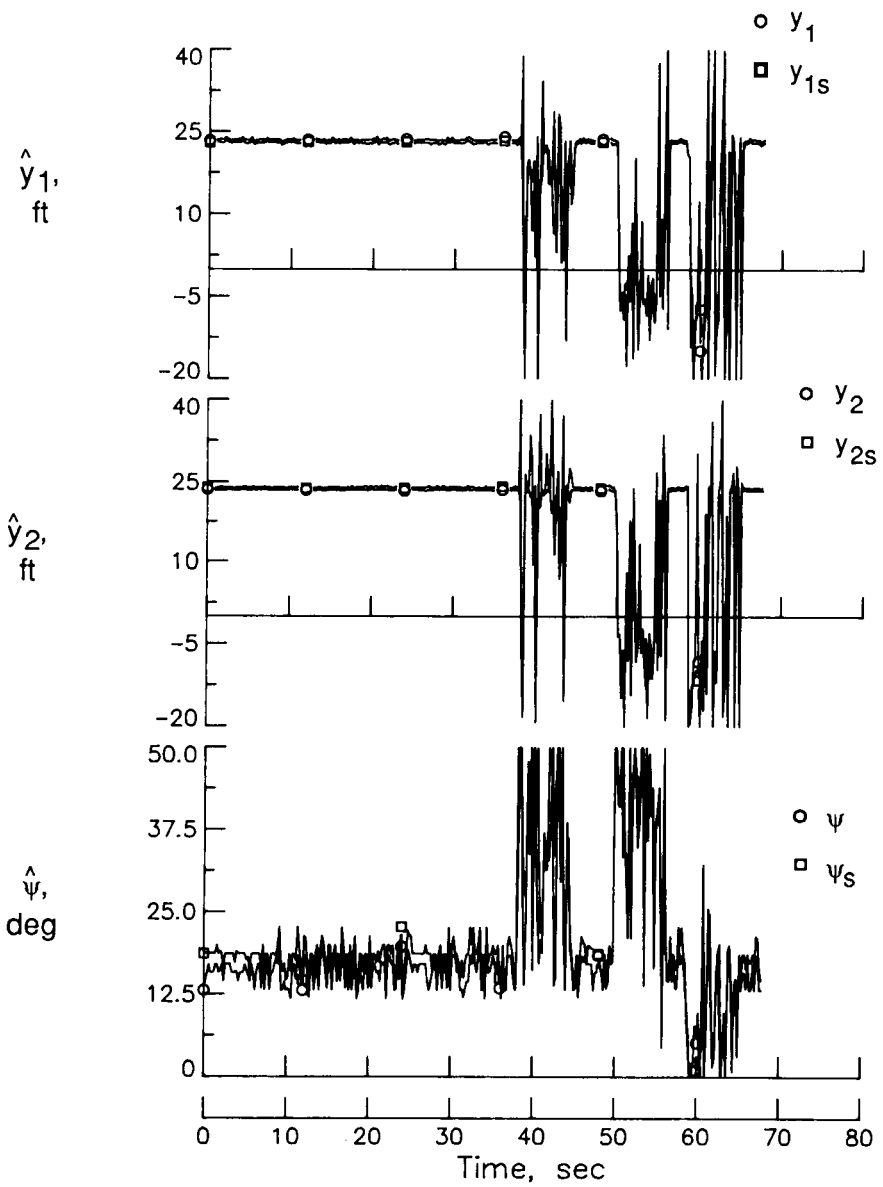

Figure 22. Concluded.

5. The system performed better at 150 Hz than at 990 Hz, but 150 Hz may not be the optimum frequency. Differences in performance between the high-Q and low-Q filters were insignificant at 150 Hz, but were very significant at 990 Hz.

6. Both $\hat{y}_1$ and $\hat{y}_2$ are adequate for moderately accurate measurement of aircraft displacement, and differences between them are small.

Based on the results of these open-loop tests, measurement of aircraft lateral displacement from centerline provided by the MLC system appears to be adequate for use by an automatic control system during roll-out, turnoff, and taxi, and future closed-loop testing of the system as part of an automatic roll-out and turnoff system is warranted.

NASA Langley Research Center
Hampton, VA 23665-5225
August 25, 1989

References

1. Hammond, A. F.: *Guidance and Control of Aircraft Ground Movement at Airports During Restricted Visibility—A Survey of Requirements and Possible Systems.* Tech. Rep. No. 65071, British Royal Aircraft Establ., Mar. 1965.
2. Morgan, H. C.; and England, P.: *A Taxi-Guidance System for Aircraft Using a Single Magnetic Leader Cable.* Tech. Rep. No. 66065, British Royal Aircraft Establ., Feb. 1966. (Available from DTIC as AD 800 204.)
3. Pines, S.; Schmidt, S. F.; and Mann, F.: *Automated Landing, Rollout, and Turnoff Using MLS and Magnetic Cable Sensors.* NASA CR-2907, 1977.
4. Pines, Samuel: *Terminal Area Automatic Navigation, Guidance, and Control Research Using the Microwave Landing System (MLS). Part 1—Automatic Rollout, Turnoff, and Taxi.* NASA CR-3451, 1981.
5. Bundick, W. Thomas: *Effects of Cable Geometry and Aircraft Attitude on the Accuracy of a Magnetic Leader Cable System for Aircraft Guidance During Rollout and Turnoff.* NASA TP-1978, 1982.
6. Young, James C.; Bundick, W. Thomas; and Irwin, Stewart H.: *Results from Tests, With Van-Mounted Sensor, of Magnetic Leader Cable for Aircraft Guidance During Roll-Out and Turnoff.* NASA TP-2092, 1983.

NASA
National Aeronautics and Space Administration

Report Documentation Page

1. Report No.	2. Government Accession No.	3. Recipient's Catalog No.
NASA TM-4135		

4. Title and Subtitle	5. Report Date
Results of Aircraft Open-Loop Tests of an Experimental Magnetic Leader Cable System for Guidance During Roll-Out and Turnoff	February 1990
	6. Performing Organization Code
7. Author(s)	8. Performing Organization Report No.
W. Thomas Bundick, David B. Middleton, and William L. Poole	L-16574
	10. Work Unit No.
9. Performing Organization Name and Address	505-66-41-04
NASA Langley Research Center Hampton, VA 23665-5225	11. Contract or Grant No.
	13. Type of Report and Period Covered
12. Sponsoring Agency Name and Address	Technical Memorandum
National Aeronautics and Space Administration Washington, DC 20546-0001	14. Sponsoring Agency Code

15. Supplementary Notes

Programming support was provided by Jessie Yeager, PRC Kentron, Inc., Aerospace Technologies Division, Hampton, Virginia.

16. Abstract

An experimental magnetic leader cable (MLC) system designed to measure aircraft lateral displacement from centerline and heading relative to centerline during roll-out, turnoff, and taxi was tested at NASA's Wallops Flight Facility using NASA's Transport System Research Vehicle (TSRV), a modified Boeing 737. The MLC system consisted of ground equipment that produced a magnetic field about a wire along the runway centerline and equipment in the aircraft that detected the strength and direction of this field and computed displacement and heading. Results of these tests indicate that estimates of aircraft displacement from centerline produced by the magnetic leader cable system appear to be adequate for use by an automatic control system during roll-out, turnoff, and taxi. Estimates of heading, however, are not sufficiently accurate for use, probably because of distortion of the magnetic field by the metal aircraft.

17. Key Words (Suggested by Authors(s))	18. Distribution Statement
Automatic landing Roll-out Turnoff Magnetic leader cable Guidance systems	Unclassified—Unlimited Subject Category 04

19. Security Classif. (of this report)	20. Security Classif. (of this page)	21. No. of Pages	22. Price
Unclassified	Unclassified	38	A03

For sale by the National Technical Information Service, Springfield, Virginia 22161-2171